Analysis of Power System Transients using Measurement-based Wideband Models

Sufia Khalid

Delft University of Technology

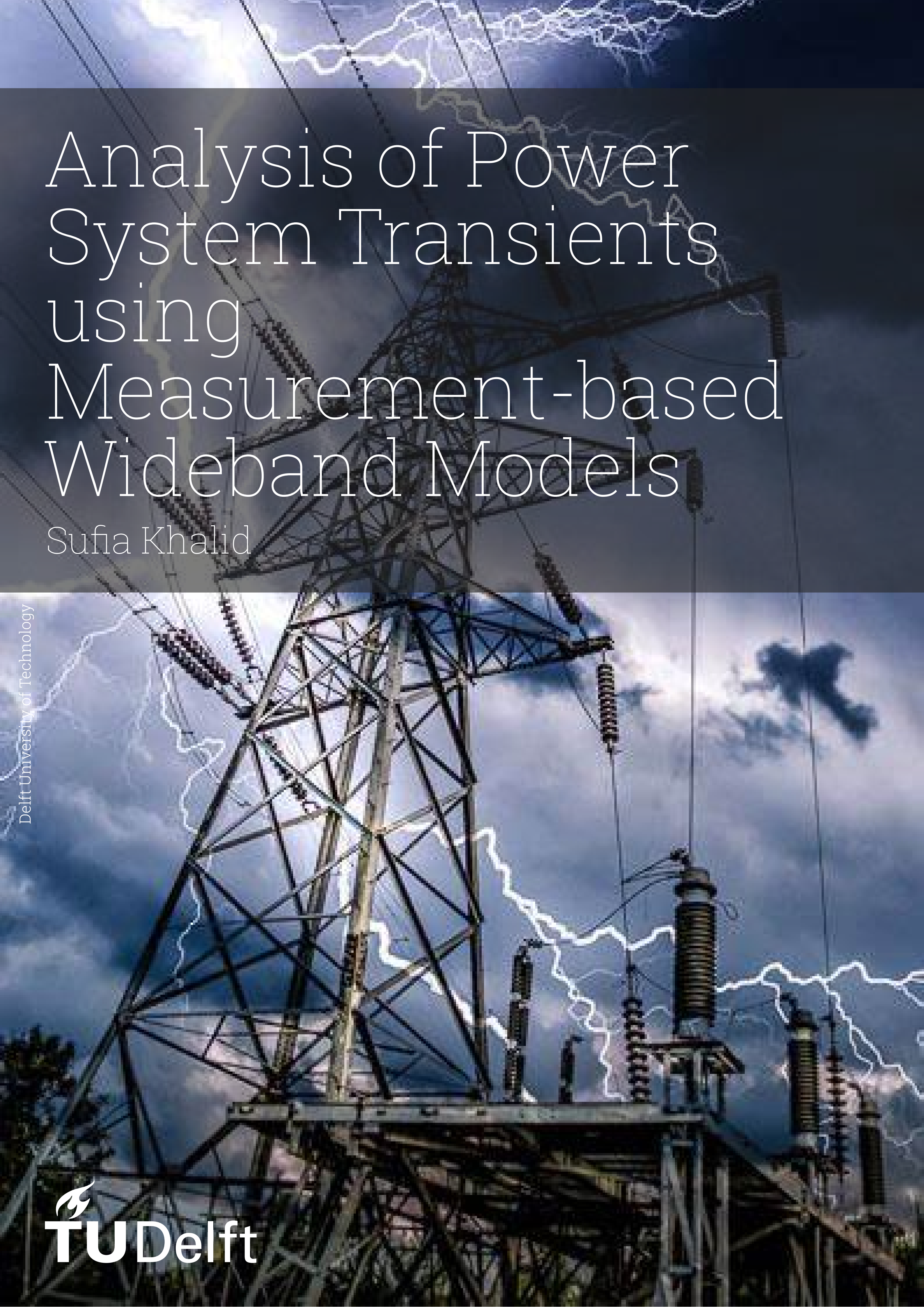

Analysis of Power System Transients using Measurement-based Wide-band Models

by

Sufia Khalid

To obtain the degree of Master of Science in Sustainable Energy Technology at the Delft University of Technology, to be defended publicly on Monday, April 28, 2025, at 12:00.

Student number:	5021413
Supervisor:	Prof.Dr.Ir. Marjan Popov
Thesis Committee:	Prof.Dr.Ir. Marjan Popov
	Assoc. Prof.Dr. Ir. Mohamad Ghaffarian Niasar
Project Duration:	April, 2024 - April, 2025
Faculty:	Electrical Engineering, Mathematics and Computer Science (EEMCS), Delft

Cover: Canadarm 2 power system under CC BY-NC 2.0 (Modified)
Style: TU Delft Report Style

TU Delft

"Electric power is everywhere present in unlimited quantities and can drive the world's machinery without the need of coal, oil, gas, or any other of the common fuels."

— **Nikola Tesla**

Preface

This thesis reports the culmination of my academic endeavors at the Delft University of Technology. Embarking on the sustainable energy technology program, I was initially drawn up with a fascinating research area of intelligent power electrical grids. However, following explorations into the profile course program of sustainable energy technology and the completion of a master's thesis, I discovered that my primary interest lies in transient studies of the power system that I consider great and immediate relevance to society. I am grateful for the friendships and opportunities that shaped me into the person I am today, both within and outside the university. I remember my student days as vibrant and filled with invaluable learning experiences. Most importantly, I would like to thank my supervisors Dr. Ir. Marjan Popov , your exceptional expertise in intelligent power grids, has been a continuous source of inspiration for me, and I appreciate your invaluable guidance and ability to connect me with the right people.Furthermore,I would like to thank Phd student Behzad Behdani for helping in developing black box model of transformer . Special thanks goes to my brother, whose love and continuous support have been a driving force behind my success, both professionally and in my personal life. Ir. Muhammad Mustafa, thank you for your belief in me, your encouragement felt welcome. Furthermore, I want to recognize and express my heartfelt thanks to my parents. Without your unconditional love and support in every way, I would never have reached where I am today. Finally, I thank Nadeem Ahmad, Yasmin, Tabassum, Mirha, Inara, Daniya, Amayra, Umaid, David Munoz, Isabella, Aatie, and Hannia Sanchez for their unwavering support.

Sufia Khalid
Hague, April 2025

Abstract

This thesis investigates switching transients in a test system comprised of a single-core underground cable, vacuum circuit breaker, and (Y-Y) star transformer. This work presents six scenarios in which test systems are connected to the transformer in different load scenarios such as no-load, medium and high loads, low and high capacitance, and a combined impedance-capacitance case. Monte Carlo simulations have been employed to introduce random variability into the parameters of vacuum circuit breaker(VCB) to enable probabilistic analysis of extreme transients. Using EMTP and MATLAB software, the study confirms how probabilistic transient analysis can be utilized to improve power system reliability and design protective switchgear.
Keywords: **Power system transients, switching over-voltages, Monte Carlo simulation, vacuum circuit breaker, transient recovery voltage, impedance-capacitance effects, electromagnetic transient simulation, EMTP modeling.**

Contents

List of Figures

List of Tables

Nomenclature

Abbreviations

Abbreviation	Definition
AC	Alternating Current
EMTP	Electromagnetic Transients Program
VCB	Vacuum Circuit Breaker
Y-Y	Star-Star Transformer Configuration
LV	Low- voltage
HV	High-voltage
TRV	Transient Recovery Voltage

Symbols

Symbol	**Quantity**	**Unit**
V	Voltage	Volt (V)
I	Current	Ampere (A)
R	Resistance	Ohm (Ω)
X	Reactance	Ohm (Ω)
Z	Impedance	Ohm (Ω)
C	Capacitance	Farad (F)
L	Inductance	Henry (H)
P	Active Power	Watt (W)
Q	Reactive Power	Volt-Ampere Reactive (VAR)
S	Apparent Power	Volt-Ampere (VA)
f	Frequency	Hertz (Hz)
t	Time	Second (s)
ω	Angular Frequency	Radian per second (rad/s)
ϕ	Phase Angle	Degree ($^\circ$) or Radian (rad)
kV	Kilovolt	1,000 Volts (V)
A	Ampere (Current)	Ampere (A)
μF	Microfarad (Capacitance)	10^{-6} Farad (F)
H	Henry (Inductance)	Henry (H)
ms	Millisecond (Time)	10^{-3} Second (s)
p.u.	Per Unit	(Unitless, normalized)
kA	Kiloampere	1,000 Amperes (A)

Table 2: List of Symbols and Units

Chapter 1

Introduction

Electrical energy plays a crucial role in a contemporary society. It is integrated with the power system through its generation, transmission, and distribution for reliable delivery to customers in residential, commercial, and industrial sectors. There is a growing body of literature [1], [2], [3], [4] that recognizes that the power system operation is significantly affected (in terms of system stability, reliability, and durability of equipment) by the injection of switching transients into the system. These transients entail detrimental effects on the power system's costly and critical components, such as power transformers, due to abrupt changes in voltages and currents. Currently, electrical power systems are experiencing a substantial paradigm shift towards renewable energy sources. The intermittent nature of these sources gives rise to more frequent switching operations in the network. In addition, more complex equipment is being integrated into the network as the energy transition progresses. Therefore, it has become an urgent necessity to address switching transients through advanced modeling techniques such as wide-band models [5]. This modeling approach provides more accurate predictions of system behavior, enabling better design and operation of future power networks and equipment.

1.1 Introduction

This thesis investigates switching transients due to synchronized contact opening of vacuum circuit breaker (VCB) . To such an aim, investigations are performed on a 40 kV test system consisting of a dry resin power transformer(Y-Y) connected to a single core underground cable and vacuum circuit breaker , implemented in the Electromagnetic Transients Program (https://emtp.com/) environment. In the developed test system, a wide-band black-box model of a real three-phase (Y-Y) power transformer is developed through accurate measurements in the laboratory. The black-box transformer model is developed based on the measurements on the high-voltage (HV) side, considering different impedance values on the low-voltage (LV) side. Accordingly, six loading conditions (Scenario Z_{nl} - $Z_{12\Omega}||Z_{3.3\mu F}$) are developed to capture a wide range of operating conditions and transient behaviors. These loading scenarios are given as follows:

1. **No-Load Scenario (Z_{nl})** : Represents the no-load condition, serving as the reference or baseline scenario for comparison.
2. **Moderate Load Scenario ($Z_{56\Omega}$)** : It simulates a system where a power transformer(Y-Y) is connected to a moderate resistive impedance of $56\,\Omega$.
3. **High Load Scenario ($Z_{12\Omega}$)** : It reflects a star-star transformer connected to a lower system impedance of $12\,\Omega$, representing higher load conditions.
4. **Low Capacitance Scenario ($Z_{0.047\mu F}$)** : It introduces a small capacitance ($0.047\,\mu\mathrm{F}$) to model minimal capacitive effects, such as parasitic capacitance.
5. **High Capacitance Scenario ($Z_{3.3\mu F}$)** : It features a significantly higher capacitance ($3.3\,\mu\mathrm{F}$) to simulate dominant capacitive effects, such as those from long cables or power factor correction.

6. **Composite Impedance-Capacitance Scenario ($Z_{12\Omega}||Z_{3.3\mu F}$)** : It Combines a resistive load ($12\,\Omega$) parallel with high capacitance ($3.3\,\mu\mathrm{F}$), representing a realistic mixed-condition model.

The key objectives of the research are that the baseline Scenario (Z_{nl}), which corresponds to the no-load condition, is utilized as a benchmark to assess the influence of various configurations concerning impedance and capacitance on the switching transients through a stochastic(Monte-Carlo) analysis approach. Some useful comparison parameters for transient over-voltage include peak transient voltage and current, waveform characteristics, and propagation dynamics. It can be noted that comparing scenarios such as Moderate Load Scenario ($Z_{56\Omega}$) and High Load Scenario ($Z_{12\Omega}$) with the no-load (Baseline) scenario provides insight as to how load increase (lower impedance) may impact transient amplitudes and durations. Similarly, the impact of capacitance, by assessing Scenario Low Capacitance Scenario ($Z_{0.047\mu F}$) and Scenario High Capacitance Scenario ($Z_{3.3\mu F}$) with respect to no-load (baseline) scenario, is included, indicating the potential for the capacitance to dampen or exacerbate the oscillatory behavior and influence the decay rates of the transients. The composite Impedance-capacitance scenario ($Z_{12\Omega}||Z_{3.3\mu F}$), the most complex, combines both the resistive and capacitive components to offer insights into practical situations where mixed impedance and capacitive effects are prevalent. All scenarios, compared with the no-load (baseline) scenario, elucidate key features of the system's transient behavior, such as the interplay of impedance, capacitance, and frequency-dependent effects. These conclusions are essential for the development of efficient system design solutions. It is to be noted that in systems with high capacitive or composite load, protective measures are needed to mitigate the transients. For this research study, a 40 kV test system is realized using EMTP software, comprising a vacuum circuit breaker, a single-core underground cable, and a dry resin type power transformer(Y-Y). The findings of this study highlight the role of detailed modeling and analysis in enabling reliability and safety across different operating conditions.

This chapter discusses the power system transients within a context and their importance, followed by explaining in detail the background, problem statement, rationale, scope, and research significance. Finally, the organization of this thesis is outlined.

1.2 Background

The power system is the backbone of today's society, transmitting electricity to homes, industries, and other services. Due to switching actions (i.e., energization of the transformer, circuit breaker operation, and fault isolation), transient OVs prevail in the system, threatening the efficient operation of the power system. In most cases, these operations cause a risk of injecting switching transients into the power system network and hindering the functionality and security of the system. According to IEEE standards, "A switching transient is described as short-duration highly damped, oscillatory over-voltage, with a duration of few milliseconds or less and occurred due to operation of the switching devices such as circuit breakers and switches" [6] . These transients can cause equipment damage, power quality issues, and sometimes system-wide outages. Hence, comprehensive study and mitigation of switching transients are of utmost importance for power system stability and reliability.

Switching transients are characterized by the abrupt change in voltage and current. These transients result from rapid fluctuations of system parameters during switching actions and can have serious impacts on power system devices. High-frequency transients can cause insulation breakdown in transformers and cables and electromagnetic interference to neighboring equipment, so proper measures are required to ensure the longevity of the power system network.

Accurate modeling and simulations are the basis for studying switching transients.

Such an approach uses advanced wide-band cables and transformer models that reflect the frequency-dependent behaviors and parasitic effects that can be valuable for transient response studies. Yet, the challenges remain in modeling systems with complex impedance and capacitance layouts, where the usual modeling techniques fail to perform [7] . This is where the need for exact simulation tools and methodologies is paramount.

This thesis investigates the switching transients in power systems using the Electromagnetic Transients Program (EMTP) software package. In this work, EMTP was used because of its superior ability to simulate electromagnetic transients in high-fidelity detail, especially for systems that involve frequency-dependent components like underground cables and transformers.[8] Furthermore, wide-band modeling and stochastic analysis within the framework of EMTP are powerful tools for investigating the complex interaction of system components under various switching conditions. This study aimed to assess the test system, which includes a voltage source of 40 kV, a vacuum circuit breaker, a wide-band underground cable model, and a star-star transformer model. Six scenarios are developed for analyzing the switching voltages, in which a wide-band model of the transformer has different sets of impedance under varying switching conditions. The findings in this research will help to compare and evaluate the transient responses obtained from different impedance configurations of the wide-band model of the transformer. This research objective is to identify key factors influencing transient behavior and propose effective mitigation strategies. The results of this observational study provide comprehensive knowledge about the switching transients and contribute to the design of more resilient power systems, providing insights that are especially useful for the wider dissemination of advanced modeling tools, such as EMTP.

Software	Key Features	Strengths	Limitations	Relevance to Study
PSCAD/EMTDC	Time-domain transient analysis; Intuitive GUI	Easy to use; Ideal for small systems	Limited wideband modeling; Less suitable for high-frequency effects	Lacks detailed modeling for wideband phenomena.
MATLAB/Simulink	Customizable; Extensive libraries	Flexible; Widely used in academia	Requires additional effort for transient-specific setups	Limited for precise wide-band transient modeling.
ATP	Open-source; Mature transient analysis tool	Cost-effective; Large user base	Steep learning curve; Limited GUI support	Basic analysis suitable, but lacks modern features.
EMTP	Wideband modeling; Stochastic analysis	Accurate; Handles complex systems	Higher cost; Requires expertise	Ideal for analyzing frequency-dependent components and complex configurations.

Table 1.1: Comparison of Transient Analysis Software [8]

1.3 Problem Statement

The reliable operation of the power system is critically dependent on understanding and managing transients, especially those provoked by switching events. Switching transients are associated with rapid voltage and current fluctuations capable of causing equipment damage and insulation failures, which deteriorate power quality.

Significant development has been made in modeling and analyzing such transients, especially using tools like the Electromagnetic Transients Program (EMTP). [9] Nowadays, measurement-based wide-band models are used in several simulations of the high-frequency behavior of system components like cables and transformers.

Despite these advances, a research gap still exists in the understanding of the detailed behavior of switching transients under different transformer configurations. In particular, wide-band transformer models with different impedance and capacitance values are rarely considered, especially under stochastic conditions where system conditions and circuit breaker operations are varied randomly. Most of the studies conducted so far adopt deterministic approaches or single transformer configurations, which cannot effectively capture the probabilistic nature of real systems and the influence of transformer diversity on transient phenomena.

The research gap is critical to address because modern, state-of-the-art power systems have a greater reliance on proper modeling to ensure resilience under extreme events. Transformers are one such key component that is instrumental in transient propagation and mitigation. The lack of comprehensive studies on how transformer wide-band models with different sets of impedance affect transient behavior and limits the ability of engineers to design systems that are robust against variations in transformer characteristics. Furthermore, stochastic variations in switching times and system parameters add further complexity that is not captured by current deterministic models.[10]

If this research gap is not addressed, system designs might not be robust enough, there will be an increase in operational risks, and equipment damage or failure might involve higher costs. The utilization of stochastic approaches with detailed transformer modeling using the EMTP allows a further step ahead in the state of the art. It enables a deep understanding of transient behaviors under real-world conditions and enables strategies to mitigate their impacts.

Therefore, this study considers six transformer configurations in a 40 kV test system and includes stochastic variations in switching scenarios. The outcome of the work will contribute to the knowledge base on power system transients, optimize system components, and improve the overall reliability and resilience of the system.

1.4 Rationale

1.4.1 Research Aim

The presented research is devoted to the investigation of power system switching transients in a 40 kV system using a wide-band measurement-based model in EMTP. Moreover, six scenarios will be developed based on the impedance configuration at the LV side of the Y-Y wide-band transformer model. In this research, the stochastic approaches accounting for real-world uncertainties will contribute to better insight into transient phenomena and the development of superior design and reliable systems.

1.4.2 Research Objectives

The following objectives will be addressed by the study to accomplish this aim:

- **Develop and validate a wide-band measurement-based model in EMTP** : Develop and validate a scheme of simulation for the voltage source, vacuum circuit breaker, wide-band model of single core underground cable, and power transformer(Y-Y) for the adopted 40 kV test system.
- **Analyze transient behavior across multiple transformer configurations** : Closer inspection to compare the switching transient responses for six transformer wide-band models in detail to understand their characteristics and impacts.
- **Incorporate stochastic variations in the model** : Simulate the effects of probabilistic variations in switching times and system conditions to measure their effects on transient magnitudes and durations.
- **Evaluate extreme transient events** : Identification of the major influencing factors causing extreme transient events and study their variation for different transformer models under stochastic conditions.

1.4.3 Research Question

This research question revolves around the modeling and frequency-dependent response of transformers during switching transients. It discusses how using a wide-band transformer (black-box model), derived from real data, can more accurately model complex transient interactions than conventional models, especially for changing load conditions. There is a need for more accurate transient simulations in current power systems to ensure reliable operation and prevent equipment damage. Conventional transformer models do not properly explain high frequency, leading to erroneous predictions and ineffective protection design. This work bridges this gap by using more realistic models under practical conditions.

1. **How does the inclusion of a wide-band black-box transformer model influence the accuracy and fidelity of transient over-voltage prediction under various loading conditions in a developed test system during Vacuum circuit breaker switching?**

2. **How can insights from scenario-based transient recovery voltage (TRV) behavior be leveraged to guide the optimal placement and sizing of over-voltage protection devices in complex power system configurations?**

3. **How do random variations in vacuum circuit breaker switching, analyzed using Monte Carlo simulations, affect the reliability of protection systems in medium-voltage networks?**

This second research question aimed to answer the question of using TRV analysis as a design tool to optimize the application of protective equipment like surge arresters. It focuses on how different load and system configurations affect TRV profiles and how this information can be used to make strategic protection decisions. As power systems become more complex, there is a growing need for scenario-based planning for protection devices. TRVs vary significantly across different system setups, and improper protection design can lead to equipment stress or failure. This research provides a structured approach to using simulation results to improve real-world device deployment.

The third research question discusses the uncertainty in VCB operational parameters, i.e., chopping current and opening time, and its effect on system behavior and protection system reliability. Rather than relying on a single deterministic occurrence, probabilistic modeling is employed to investigate the whole range of likely possibilities. Medium-voltage protection schemes must be immune to stochastic variations in switching activity, which may produce occasional over-voltages or protection failure. These uncertainties are poorly addressed by existing deterministic techniques. Monte Carlo techniques are employed because a statistical, simulation-based methodology must be used to understand and minimize these risks.

1.5 Scope

The target of this research is the power system engineering industry, with a focus on the analysis of switching transients in high-voltage systems. The developed model, presented here, will be simulated by the Electromagnetic Transients Program. It contains a 40 kV voltage source connected through a vacuum circuit breaker to a wideband-modeled underground cable and a star-star transformer. This is further limited to the technical phenomena and operational factors that determine the magnitudes of transients in regard to system reliability by analyzing transient behaviors in this configuration under conditions of stochastic switching.

There has not been any geographical or regional focus as such, but more general insights are applicable throughout the world on power systems with underground cable networks employing advanced models of transformers. Temporally, the analysis shall be restricted to an analysis of the steady-state condition and some simulated transient conditions through certain specified operating scenarios or even stochastic variations in switching operations, for that matter, anything more wide-ranging-in that, the case of the application of different voltage levels and topologies-are not engaged so to keep this investigation focused and relevant.

The research essentially involves technical themes related to the behavior of switching transients, the role of transformer impedance characteristics, and the effect of stochastic switching phenomena on the magnitudes of the same. No broad socioeconomic or environmental concern is pursued in any depth.[11] These results of the study try to improve the insight into transient dynamics in modern power networks and underpin the development of mitigation strategies for better design and operation of high-voltage equipment.

1.6 Research Significance

The wide-band measurement-based modeling of power system transients is of paramount importance from both academic and practical standpoints. This research identifies the gap in the literature regarding transient studies in a 40 kV system with advanced modeling features: vacuum circuit breaker, wide-band modeled underground cables, and star-star transformer. Moreover, six scenarios are developed based on transformer impedance configuration such as moderate load, high load, low capacitance, high capacitance, composite impedance-capacitance, and no-load scenario. The stochastic approach used to analyze switching transients under variable operating conditions provides new insight into the understanding and mitigation strategies of transient phenomena in modern high-voltage power systems and contributes much to the theoretical understanding of electromagnetic transients.

This work enables, from an application point of view, the engineer and the system operator to explain the nature of the transient magnitude and behavior variability arising due to transformer-impedance characteristics and further leads them in designing or choosing an appropriate transformer or any other protection equipment to meet their challenge for improved reliability and strength of the power system. The stochastic modeling based on probability for the vacuum circuit breaker operations allows a prediction for extreme transient events, which in turn permits the devising of even more efficient mitigation strategies and operational protocols.

This study bridges the gap between academic theories and industrial practices by judiciously combining state-of-the-art modeling techniques with an emphasis on applicability to real-world scenarios. Based on several prior studies, this work provides a critical approach toward understanding switching transients and their contributing elements while suggesting new pathways in minimizing system performance risks from possible transient events. This work becomes highly relevant in the context of the modernization of grid infrastructure, with the increasing deployment of underground cables and advanced transformer models to sustain demand for sustainable and reliable energy systems.

1.7 Study Limitations

This research, though providing many valuable insights into the analysis of power system transients by a wide-band measurement-based model, has several areas of possible limitation. The findings were restricted to a single system configuration with a 40 kV voltage source, a vacuum circuit breaker, a wideband model of single core underground cable, and a three-phase power transformer(Y-Y). Furthermore, six scenarios are developed based on transformer impedance configuration, which include moderate load, high load, low capacitance, high capacitance, composite impedance-capacitance, and no-load scenarios. Although this is a wide configuration that captures practical scenarios, it will not represent all possible variations that may occur in real systems, including lengths, circuit breakers, and transformer models, potentially limiting the generalization of the findings.

Secondly, it analyzes the transient behaviors involving stochastic variations in switching time in breakers and operation conditions. This approach allows the quantification of transient events in terms of a probability understanding that naturally emanates from the precision and realistic character of the statistical distribution and simulation parameters used, as well as the parameters modeled from those found in real conditions [12].Moreover, the analysis does not consider environmental factors, such as temperature or humidity, which can also affect transient behavior, especially in outdoor equipment.

Finally, the use of the electromagnetic transient program (EMTP) software package as the simulation platform introduces its limitations, though it is highly effective. The accuracy of the wide-band model of the underground cable and transformer depends upon the precision of their parameterization, which may not be perfect in real-life performance. Further, there are computational limitations that may forbid the variation of parameters and simulation scenarios to be pursued to any considerable extent. These limitations are indications that the research has to be supported by further studies and experiments to consolidate the results in various situations.

1.8 Thesis Overview

The research work in this thesis is organized into five chapters, each addressing one of the key components of the research on power system transients in a wide-band measurement-based model. The chapters allow for a systematic exploration of the topic, from foundational understanding to detailed analysis and recommendations.

Chapter 1: Introduction

The introductory chapter will establish the background information, problem statement, and rationale (research aim, objective, and research questions). It shall outline the motivation for the study through the importance of understanding switching transients in power systems. This chapter will explain the limitations and scope of the research to focus on analyzing transient phenomena in the adopted test system with vacuum circuit breakers, wide-band modeled underground cable, and transformer models.

Chapter 2: Literature Review: Modeling Power System Components for Transient Simulation Studies

This chapter examines prior research and theories that address the subjects of power system transients, operations of vacuum circuit breakers, wide-band modeling techniques of transformers, and underground cables. Moreover, critical analysis identifies the knowledge gap in the literature on the stochastic analysis of switching transients. The chapter establishes the theoretical foundation for the thesis, connecting existing knowledge to the specific objectives of this research.

Chapter 3: Power System Component Development in EMTP

Chapter 3 presents the development of the system model in the Electromagnetic Transient Program (EMTP) simulation environment. This chapter provides the configuration of the test system with more detail on the modeling of the vacuum circuit breaker, wide-band underground cable, and transformer models. The transformer model is developed by considering six loading conditions replicating scenarios such as moderate load, high load, low capacitance, high capacitance, and composite impedance-capacitance. Additionally, the over-voltage performance of the test system is analyzed by defining stochastic switching scenarios.

Chapter 4: Switching Transient Analysis in a given Test System using Monte Carlo Simulation

In this chapter, Monte Carlo simulations are utilized to examine the parameter variation in the vacuum circuit breaker during switching events that influence transient recovery voltage (TRV) and transformer voltage in a test system.Moreover, Transient recovery voltage (TRV) and transformer voltage response for different transformer loadings are simulated by varying VCB parameters based on specified probability distributions.

Chapter 5: Conclusion and Future Work
The last chapter summarizes the findings and shows implications for the design of power systems and operational practices. It revisits the research objectives, discusses the limitations of this study, and gives directions for further research. Finally, some practical recommendations are made to alleviate switching transients and improve system reliability, concluding the thesis with some practical insights.

Chapter 2

Literature Review: Modeling Power System Components for Transients Simulation Studies

2.1 Introduction

Power systems transient analysis is an important field of research intended to understand the transition of electrical and magnetic energies within the components of the system subsequent to abrupt changes in the electrical network conditions. Much of the literature since the mid-1990s has emphasized the comprehensive study of transients in a power system. Allan Greenwood (1973) in his seminal work, **Electrical Transients in Power Systems**,[13] defined transients as temporary deviations in voltage and current due to sudden changes in the power system conditions such as switching operations, faults, or lightning strikes. Greenwood emphasizes the importance of understanding these transients to ensure reliability and stability in power systems. Similarly, in 2001, researcher Lou van der Sluis published his work **Transients in the Power System**,[14] in which he discussed recent developments in measurement techniques, computer modeling, and switchgear development and showed the need for advanced modeling techniques for capturing the transient characteristics that reflect the real-world situation. It is now well established from these two studies that advances in modeling, and computational techniques are required to increase the capability of analyzing and predicting transient behavior. This chapter focuses on the application and development of measurement-based wide-band models in modern power systems aimed for accurate analysis of power system switching transients during synchronized opening of vacuum circuit breaker contacts.

2.2 Switching Transients in the Power System

”Switching transients” are defined as voltage and current variations with steep front-of-wave shapes, often with oscillatory waveforms that dampen out. Such disturbances may propagate through the power networks in the form of traveling waves, reflecting and refracting at the point of impedance mismatch in the system. These transients occur in various electrical systems, including high-voltage transmission, medium-voltage distribution, and industrial installations. Different research works tried to explain the complexity of the switching transients of the power systems by studying their origin, characteristics, and effects in different contexts. An analytical approach to transients was presented by Evans, Monteith, and Witzke (1939) [1] in their research studies ”Power system transients caused by switching and fault,” which addresses over-voltages, traveling waves, and oscillations in voltage and current. This study examines the significance of system design in minimizing adverse effects and establishes the foundation for comprehending the interaction in the system component during transient events. Furthermore, another researcher in 1987, Ari and Blumer [15], came up with research work focused on the physics behind the electromagnetic field production during the time of switching transients in the power system. This research reported that the electromagnetic field spread across the system's surroundings and produced interference with adjacent equipment. Moreover, the need for safeguards like grounding and shielding to lessen electromagnetic interference was illustrated through case studies. However, Hwang and Lou's [16] application-oriented study on capacitance switching in industrial power systems in 1998 was seen as the beginning of a new era in which theoretical knowledge was not restricted to books or research projects but brought positive changes by studying switching transients in industrial sectors. In this research work, Hwang emphasizes switching device features and system parameters to shape transient behavior and proposed mitigation techniques, including pre-insertion devices and optimized switching sequences. All three findings have significant implications for the understanding of the switching transients, from theoretical and experimental approaches to modern simulation-driven solutions, addressing challenges ranging from equipment protection to electromagnetic compatibility.

2.2.1 Nature of Switching Transients

Switching transients in the power system occur during sudden system reconfiguration due to the redistribution of stored energy in the inductive and capacitive components of the power system.[17]The switching transient response is illustrated by rapid changes in both voltage and current, often with oscillatory waveforms whose amplitude is progressively attenuated due to system damping. The defining features of switching transients (high-frequency oscillations, rapid alterations in voltage and currents, and short times - by the category of switching transient). This means that each category addresses how the transient behavior can be interpreted depending on its origins, the shape of waveforms, and the interactions in systems to which they appear.[18] It can shed better light on the nature of switching transients and their impact on power systems.

1. **Based on the cause of switching Transients:**
    - **Circuit Breaker Operation**: In this case, high-frequency oscillations, and steep-fronted transients are generated due to sudden changes in the current flow. Re-ignition or restrike adds nonlinear effects and prolongs the oscillatory behavior.
    - **Capacitor Bank Switching**: It is characterized by oscillatory transients due to the interaction of the capacitor's stored energy with system inductance, producing high-frequency damped oscillations.
    - **Transformer Energization**: In this case, magnetizing inrush currents dominate the low-frequency oscillatory transients, which frequently involve the nonlinear saturation effects of the core.

- **Underground Cable Switching**: Distributed capacitance and inductance of the cable cause high-frequency transients, while traveling wave effects cause reflection and refraction at underground cable terminations.
- **Fault Clearing:**: It creates steep-fronted and oscillatory transients, such as transient recovery voltage (TRV), with high over-voltages and rapid energy redistribution.

2. **Based on Waveform Characteristics of Switching Transients:**
   - **Oscillatory Transients**: Interaction between inductive and capacitive elements causes sustained oscillations that gradually decay. These transients commonly occur in capacitor bank and transformer switching.
   - **Unidirectional Transients**: These types of switching transients give rise to sharp, single-pulse waveforms with high amplitude, typically originating from fault clearing or lightning-induced events.
   - **Steep-Fronted Transients**: These transients constitute high-frequency voltage/current changes with fast rise times, seen during fast switching or external disturbances like lightning strikes.

2.2.2 Key Characteristics of Switching Transients

Switching transients are complex electrical phenomena that occur at sudden changes in the state of operation of a power system. Their important characteristics include:

1. **High-Frequency Components**: Switching transients frequently involved high-frequency oscillations, usually in the kilohertz to megahertz range. These frequencies arise due to the interaction between inductive and capacitive components in the system.
2. **Short Duration**: The duration of switching transients ranges from a few microseconds to milliseconds. Even though they are brief, they can majorly impact system stability and equipment.
3. **Steep Voltage and Current Variations**: Voltage and current fluctuate quickly during switching transients, which frequently have steep wave-fronts. This feature makes protective devices and insulation challenging.
4. **Oscillatory Behavior**: Most switching transients are oscillatory, with energy switching between capacitive and inductive components, and system resistances usually cause these oscillations to become damped over time.
5. **Traveling Wave Phenomena**: Transients travel along transmission lines and cables as traveling waves, and impedance mismatches result in reflections and refractions, which affect the transient's magnitude and waveform.
6. **Overvoltages**: Switching transients frequently cause overvoltages that are higher than typical operating values, which can strain equipment insulation and cause failure.
7. **Nonlinear Effects**: Switching transient waveforms can be shaped by nonlinear phenomena, such as arc re-ignition in circuit breakers. These transients become more complicated and unpredictable as a result of these impacts.

2.3 Measurement-Based Wide-band Model

Measurement-based wide-band modeling has become one of the most important approaches to investigating the high-frequency transient behavior in electrical systems, in particular for underground cables, power transformers, and circuit breakers. In this approach, measured data are used to obtain a representation of system behavior that is accurate within a wide frequency range, with high accuracy for high-frequency transient studies.[19]

They also become indispensable during transient analysis, as they capture a system's response due to a broad spectrum of frequencies, including the kind of frequencies developed by fast-switching events, electromagnetic interferences, and lightning strike events. Traditional models are narrow-band or lumped-parameter models that poorly capture these dynamics and fail to correctly predict transient behavior. Wide-band models eliminate these limitations by considering the resistances, inductances, capacitances, and conductances as frequency-dependent parameters.[20]

Unlike purely analytical or simulation-based models, measurement-based wideband models draw upon empirical data actually obtained from laboratory or field measurements. This approach ensures that the model reflects real-world conditions, including complex interactions and imperfections not easily captured by theoretical methods. The primary steps in developing a measurement-based model include:

1. **Measurement Setup**: The voltage/current signals in impulse or sinusoidal nature are injected into a system, and the respective system response is recorded with high-frequency equipment. Time Domain Reflectometry (TDR) and Frequency Network analyzers such as the Bode analyzer are the most conventional tools used in this practice.
2. **Parameter Extraction**: The process of extracting frequency-dependent parameters from the measured data is often carried out via techniques like vector fitting, rational approximation, or Prony analysis. In this study, the vector fitting method is applied, which will be introduced further.
3. **Model Validation**: The parameters extracted are then used to construct a model, which may be validated against other measurement data or known benchmarks.

In the next section, the fundamentals of transformer, underground cable, and vacuum circuit breaker modeling will be discussed to attain a prior understanding of electrical principles before developing wide-band models for power system components.

2.4 Fundamentals of Transformer Modeling

Transformer modeling is an essential step prior to simulation for the sake of understanding power transformer behavior under different situations, especially those associated with electromagnetic transient events. The main approaches towards modeling power transformers are divided into two categories: 1) detailed internal winding models and 2) terminal-based models. The internal winding models consider the details in the physical and geometric areas of transformer windings by solving field problems for the accurate facilitation of distributed inductance capacitance and mutual coupling. While these models give insight into internal stresses and initial voltage distributions, their complexity and high computational requirements make them impractical for system-level studies. In contrast, terminal models simplify the representation by focusing on the electrical behavior observed at the transformer's external terminals. The same holds true for electromagnetic transient studies where high-frequency effects such as stray capacitance and frequency-dependent losses dominate.[21] The terminal model captures the input-output relations of the transformer in terms of measurable parameters and, therefore, is a practical and computationally efficient means to include transformer dynamics in system simulations.

2.4.1 Transformer Terminal Model

The terminal transformer model represents the transformer's behavior in terms of its admittance matrix (Y) at the terminals. It captures the relationship between terminal voltages and currents, which is frequency-dependent, thereby giving an accurate representation of transformer dynamics over a wide frequency range. The Y-matrix can be derived through frequency-domain measurements or calculated based on the transformer's design and construction details. The calculated admittance functions are approximated by rational functions, from which equivalent RLC networks suitable for time-domain simulation tools can be created.[20]The key strength of this approach is its capability to capture the transient response of a power transformer for which internal details of its geometries are not well known. By focusing on the behavior seen from its terminals, this modeling technique can be employed to model various types of power transformers, expanding to even multi-winding, multi-phase structures. The terminal model accounts for frequency dependency effects: core losses, stray capacitance, resonance phenomena extracting important over-voltages, harmonic propagation, and EMI predictions. Moreover, enforcing passivity in its approach ensures that the model remains stable during simulations, preventing non-physical results.

Figure 2.1: A Four terminal model of Transformer [20]

The terminal model of the transformer is widely used in the development of wide-band models, mainly for transient analyses that include studies on switching transient, propagation of lightning surge, and high-frequency resonances. It provides insight into incorporating the transformer in overall system-level simulation without losing accuracy at higher frequencies. Unlike the internal winding models that are computationally intensive and need access to proprietary design details, the terminal models, on the other hand, are practical and flexible; they can act in a standalone manner or as an add-on module within a comprehensive model. Therefore, these models represent the preferred choice for engineers with an interest in the balance of accuracy and computational efficiency for power system transient studies.

2.4.2 Admittance Matrix Representation

The Admittance Matrix Representation provides a compact and systematic way to describe the relationship between a transformer's terminal voltages and currents. [22] It captures the wide-band, frequency-dependent behavior of the transformer as seen from its terminals. This is especially useful for modeling and simulating electromagnetic transients and high-frequency responses in power systems.
The relationship is given by:

$$I = Y.V \tag{2.1}$$

I: A column vector of currents at the transformer terminals ($n \times 1$).
V: A column vector of voltages at the transformer terminals ($n \times 1$).
Y: The admittance matrix ($n \times n$), which relates the terminal currents and voltages.
n: The number of considered terminals.
The admittance Y is complex in nature and includes both real (conductance) and imaginary (susceptance) components. Furthermore, it is symmetric, which implies Y_{ij}=Y_{ji}, due to the reciprocity of transformer components. For a multi-winding transformer with n terminals, the Y matrix is composed of

1. Self Admittance/Diagonal Elements (Y_{ii}): This matrix represents the admittance of each terminal with respect to ground. In addition, effects like leakage inductance, core losses, and stray capacitances are included.
2. Self Admittance/Off diagonal Elements (Y_{ij}): It represents the interaction, or coupling, between different terminals and accounts for mutual inductance and capacitive coupling between windings.

In the transformer, the elements of the admittance matrix are frequency-dependent: At low frequency, the transformer behaves inductive, dominated by leakage inductance and core losses. On the other hand, at high frequencies, stray capacitances become significant and thus result in a predominantly capacitive behavior.[23]

2.4.3 Rational Function Approximation

In order to implement the frequency-dependent model in EMTP software for further analysis, the elements of the Y-matrix should approximated using rational functions:

$$Y(s) = \sum_{k=1}^{N} \frac{r_k}{s - p_k} + d \tag{2.2}$$

where:
s: Complex frequency variable.
r_k: Residues associated with each pole.
p_k: Poles representing the frequency-dependent characteristics.
d: Constant term accounting for high-frequency asymptotic behavior.

This approximation will be taken by the frequency-domain Y-matrix through the fitting of measured or calculated wide-band admittance data. An essential step here is the representation using the rational function, considering the requirements of the EMTP algorithm. Time-domain simulation of frequency responses in EMTP is carried out in two ways: i) based on an equivalent RLC network, or ii) calculating the convolution of the system's transfer function by the desired input through the recursive convolution algorithm. In either case, the measured frequency response should first be approximated by rational functions. That would make it possible to get accurate modeling for transient and high-frequency phenomena, maintaining computational efficiency and numerical stability.

2.4.4 Equivalent Circuit Representation

The approximation of the frequency-dependent response with rational functions allows for the realization of a basic equivalent circuit with RLC components, where each term in the approximation corresponds to a specific branch in the circuit.[20]This allows for better modeling of complex electromagnetic systems using simpler passive components. A pole as a single term in the rational function approximation, p_k, can be implemented either by an RL or RC branch in the equivalent circuit. On the other hand, a pair of complex conjugate poles in the approximation corresponds to an RLC branch in the equivalent circuit.[17]Such a branch can model resonant behavior in the system.

2.4.5 Nodal Admittance Representation

In a multi-phase transformer, the terminal relationships can be expressed using the nodal admittance matrix:

$$\begin{bmatrix} I_1 \\ I_2 \\ \dots \\ I_n \end{bmatrix} = \begin{bmatrix} Y_{11} & Y_{12} & \dots & Y_{1n} \\ Y_{21} & Y_{22} & \dots & Y_{2n} \\ \vdots & \vdots & \vdots & \ddots \\ Y_{n1} & Y_{n2} & \dots & Y_{nn} \end{bmatrix} \times \begin{bmatrix} V_1 \\ V_2 \\ \dots \\ V_n \end{bmatrix} \tag{2.3}$$

Modal Decomposition

The modal decomposition of the admittance matrix (Y-matrix) is expressed as:

$$Y_{modal} = T^{-1} Y T \tag{2.4}$$

where,
Y is the original admittance matrix
T is the transformation matrix
Y_{modal} is the modal admittance matrix

The main purpose of modal decomposition is the decoupling of the system into independent modes; the system, in a modal domain, can be treated as an uncoupled single-phase circuit. This will substantially reduce the computational complexity, particularly for large systems.

2.5 Fundamentals of electrical cable modeling

2.5.1 Transmission line equation

The electromagnetic behavior of transmission lines and cables is [24]described by the Telegrapher Equations, which in frequency domain are as follows:

$$\frac{d\mathbf{V}}{dx} = -\mathbf{ZI} \tag{2.5}$$

$$\frac{d\mathbf{I}}{dx} = -\mathbf{YV} \tag{2.6}$$

where $\mathbf{V}$ is the vector of line phase voltages, $\mathbf{I}$ is the vector of phase currents, $\mathbf{Z}$ is the series impedance matrix in per unit length, and $\mathbf{Y}$ is the shunt admittance matrix also in per unit length. It is worth mentioning that uppercase letters are used here to indicate frequency-domain variables, lowercase letters represent time-domain variables, and boldface letters represent matrix and vector quantities.
The general solution of (2.5) and (2.6) for the vector of currents is [25]:

$$\mathbf{I(x)} = e^{-\psi x}\mathbf{C_1} + e^{\psi x}\mathbf{C_2} \tag{2.7}$$

where $\mathbf{C_1}$ and $\mathbf{C_2}$ are vectors of integration constants and $\psi = \sqrt{YZ}$ is the propagation matrix. A solution for the voltage in terms of the same constants is derived by replacing (2.7) in (2.6), as:

$$\mathbf{Y_c V(x)} = e^{-\psi x}\mathbf{C_1} + e^{\psi x}\mathbf{C_2} \tag{2.8}$$

where Y_c is the matrix of characteristic admittances:

$$\mathbf{Y_c} = \left(\sqrt{\mathbf{YZ}}\right)^{-1} \tag{2.9}$$

2.5.2 Transmission Line Model

Consider now a line segment of length $x = l$, as the one shown in Figure 2.2. Evaluating (2.3) and (2.4) at $x = 0$, the following is obtained:

$$I(0) = I_0 = C_1 + C_2 \tag{2.10}$$

$$Y_c V_0 = Y_c V_0 = C_1 - C_2 \tag{2.11}$$

By integrating, the constant vectors can be expressed as follows:

$$C_1 = (I_0 + Y_c V_0)/2 \tag{2.12}$$

$$C_2 = (I_0 - Y_c V_0)/2 \tag{2.13}$$

Now, (2.7) and (2.8) are determined at $x = l$:

$$I(l) = -I_l = e^{-\psi L}C_1 + e^{\psi L}C_1 \tag{2.14}$$

$$Y_c V(l) = Y_c V_l = e^{-\psi L}C_1 + e^{\psi L}C_1. \tag{2.15}$$

In (2.14), the currents entering a line are taken as positive. From equation (2.14) and (2.15), the following is obtained:

$$I_l - Y_c V_l = -2e^{-\psi L}C_1, \tag{2.16}$$

and from (2.12),

$$I_l - Y_c V_l = -H(I_0 + Y_c V_0) \tag{2.17}$$

with,

$$H = e^{-\psi L}. \tag{2.18}$$

This matrix is called the propagation factors matrix. The current of the line terminal at $x = l$ is expressed by (2.17). A companion expression can be written to represent the line terminal current at $x = 0$, as follows:

$$I_0 = Y_c V_0 = -H(I_l + Y_c V_l) \tag{2.19}$$

Based on the aforementioned equations, one can consider a vector of currents in a transmission line that are reflected at $x = 0$ and move in the direction of the terminal at $x = l$. To motivate the fact C_1 is denoted as I_{0r} (2.16), the following can be written:

$$I_l = Y_c V_l - 2HI_{0r} \tag{2.20}$$

Likewise, a vector of currents reflected at $x = l$ and moving in the direction of $x = 0$ is perceived based on equation (2.13), as well.[26] Regarding the indication of C_2 by I_{lr} in (2.19), the following holds:

$$I_0 = Y_c V_0 - 2HI_{lr} \tag{2.21}$$

These statements apply to both aerial lines and underground/submarine cables and provide the foundation of the wideband cable model.[27]

2.5.3 Nodal Form of Line Model

Expressions (2.17) and (2.19) can be formulated and grouped in the following way:

$$\begin{bmatrix} U & H \\ H & U \end{bmatrix} \times \begin{bmatrix} I_l \\ I_0 \end{bmatrix} = \begin{bmatrix} Y_C & -HY_c \\ -HY_c & Y_C \end{bmatrix} \times \begin{bmatrix} V_l \\ V_0 \end{bmatrix} \tag{2.22}$$

where U is the unit matrix.

2.6 Fundamentals of circuit breaker modeling

A circuit breaker is a switch that ensures the reliable interruption of operating and short circuit currents within electrical power systems. Additionally, it should also ensure the safe insulation of the recovery voltage. In most CB technologies, the arcing current is extinguished at the current zero crossing when the insulating distance between contacts for the necessary dielectric strength is attained.[28]This necessity is reached either by cooling or when the arcing inception voltage has increased enough.

Due to the different voltage levels and applications, the following different technologies have been developed:

- Air Blast Circuit Breaker (ACB)
- Vacuum Circuit Breaker (VCB)
- Bulk Oil Circuit Breaker
- Minimum Oil Circuit Breaker

- SF_6 Circuit Breaker

Vacuum circuit breakers are so far established in high voltage technology for networks below 100 kV. Since they had been used for the analyses carried out in this thesis, they are briefly described in the following section.

2.6.1 Vacuum Circuit Breakers

Vacuum circuit breakers are some of the most vital equipment in modern power systems due to their excellent arc-extinguishing properties, long service life, and low maintenance. For analyzing the behavior of the Vacuum circuit breaker during transient events and ensuring reliability with mitigation of potential issues in power system operation, accurate modeling is very much essential. Wide-band modeling has emerged as a powerful approach to accurately represent the Vacuum circuit breaker over a broad frequency range, suitable for transient analysis.

2.6.2 Fundamentals of Re-striking in Vacuum Circuit Breakers

Re-striking in a vacuum circuit breaker (VCB) occurs when the contact gap dielectric strength cannot withstand the transient recovery voltage (TRV) and hence the arc restrikes.[29] This is particularly relevant in high-frequency switching applications, where the breaker contacts' voltage oscillates due to system parameters. The restrike moment is predominantly governed by the contact opening time (t_{open}) which governs the arc quenching condition and the probability of dielectric breakdown. The most significant governing equation for re-striking voltage is:

$$V_{restrike} = L_{stray}\frac{di}{dt} + IR_{stray} + \frac{Q}{C_{stray}} \tag{2.23}$$

where,
L_{stray} is the stray inductance
R_{stray} is the stray resistance
C_{stray} is the stray capacitance
I is the current just before the interruption
Q is the charge stored in the parasitic element

2.6.3 Switching Transients During Re-striking

Re-striking causes switching transients in the system, which manifest as high-frequency oscillations with potential destructive over-voltages. System damping and natural frequency determine transient action, which is governed by:

$$f_n = \frac{1}{2\pi}\sqrt{\frac{1}{L_{stray C_{stray}}}} \tag{2.24}$$

f_n is the most common mode of oscillation. Increased stray capacitance results in lower frequency and reduced peak over-voltage, and reduced stray capacitance creates steeper, more dangerous transients. System impedance, the presence of other switching devices, and transformer magnetization properties determine the re-striking transients as well.

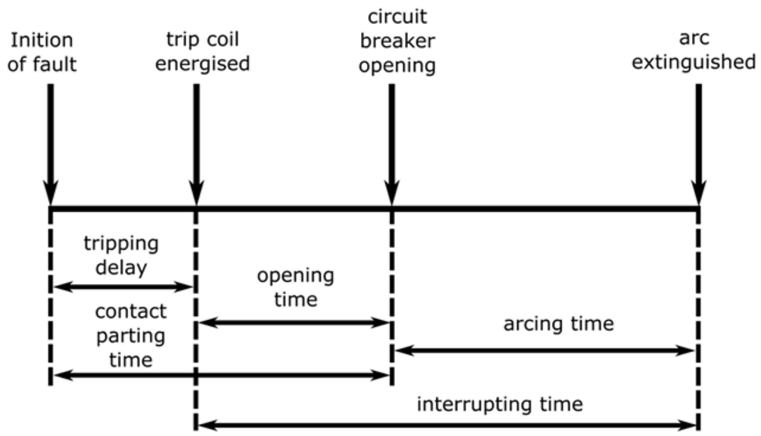

Figure 2.2: Total Fault Clearing Time [29]

2.6.4 Impact of Vacuum circuit breaker Parameters During Re-striking

The severity of re-striking is a function of vacuum circuit breaker parameters such as stray elements ($R_{stray}, L_{stray}, C_{stray}$) and transient conditions at the moment of arc extinction. The overall influence of these parameters can be described by the damping ratio (ζ), which is given by:

$$\zeta = \frac{R_{stray}}{2}\sqrt{\frac{C_{stray}}{L_{stray}}} \tag{2.25}$$

where,

- $\zeta > 1$ indicates over-damped behavior with no oscillations,
- $\zeta < 1$ results in under-damped conditions with high transient peaks.

A major outcome is that it causes more aggravated voltage oscillations and raises the natural frequency of the system. An increase in stray resistance decreases the chances of insulation breakdown by dampening the transient peaks.

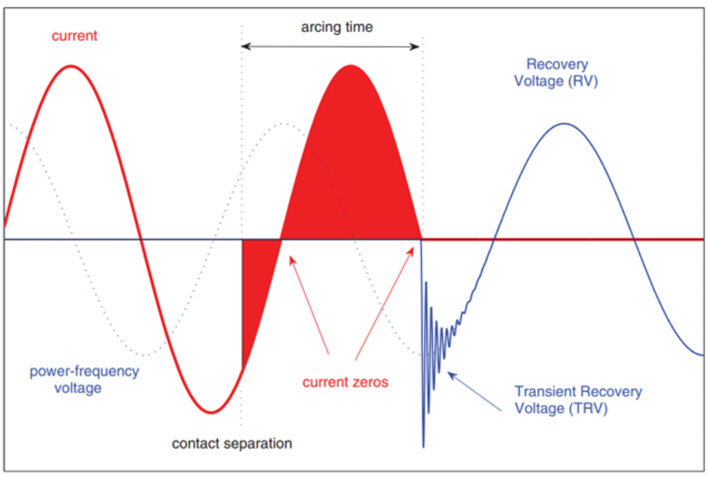

Figure 2.3: Current Interruption in a Purely Inductive AC Circuit.[29]

2.6.5 Influence of Parameters A, B, C, and D of vacuum circuit breaker in Re-striking

The re-striking transient response can be approximated by:

$$V_{trans}(t) = Ae^{-Bt}cos(Ct + D) \tag{2.26}$$

where,

- A represents the initial amplitude of the transient voltage surge.
- B defines the decay rate of oscillations.
- C corresponds to the frequency of oscillations.
- D represents the phase shift of the transient waveform.

Higher values of B (more damping) in real systems reduce unwanted oscillations, and small values of C (lower frequency) are indicative of a smooth transient response. The limiting effect on power systems can be reduced by adjusting the capacitance, inductance, and resistance of the system.

Chapter 3

Power System Component Development in EMTP

3.1 Transformer modeling-Wide band model

A Transformer Wide Band Model is a highly developed mathematical and electrical model of a transformer that very accurately represents its operation across a broad frequency band, from power system frequencies (50/60 Hz) up to high-frequency transients (in the kHz-MHz range) [20].The model has specific applications in the analysis of electromagnetic transients, switching surges, lightning impulses, and very fast transient over-voltages (VFTOs) in power systems.

This research focused on the development of a measurement-based wide-band (Black Box) model of a three-phase GEAFOL Trafo-Union 660 kVA, star-star power transformer. There is no need to rely on internal design specifics like winding configuration or core material, the black-box modeling approach for the GEAFOL Trafo-Union 660 kVA star-star transformer tries to capture its wide-band frequency-dependent response. Here, the transformer is instead treated as a dynamic system, and measurement data are used to describe the input-output relation directly. The application of this procedure is valuable for electromagnetic transient (EMT) simulation as the model accurately assesses transformer performance under all ranges of frequency and transient applications. In making such analysis possible between resonance incidents, high-level transient conditions, and switching processes, and these elements are not always simply described with the use of standard nameplate data or with design-symmetry model simulation—the black-box model serves strongly.

3.1.1 Experimental Setup and Procedure:

To obtain the Wide-band (black-box model), frequency-domain impedance and admittance measurements are taken using a Bode 100 Vector Network Analyzer. The analyzer inserts sinusoidal signals over a wide range of frequencies (from 10 Hz to a few MHz) on the high-voltage (HV) side of the transformer, with various loads connected on the low-voltage (LV) side. Other than the reference no-load condition, the loads are equivalent to 56Ω resistive, 12Ω resistive, $0.047\mu F$, $3.3\mu F$, and 12Ω in parallel with $3.3\mu F$ composite impedance. With such simulation of real operating conditions as well as transient conditions, the system guarantees both low-frequency and high-frequency responses. The study of the variation of the dynamic behavior of the

Figure 3.1: GEAFOL Trafo-Union 660 kVA, star-star power transformer

transformer with external circuits is made possible by the application of various loading conditions.

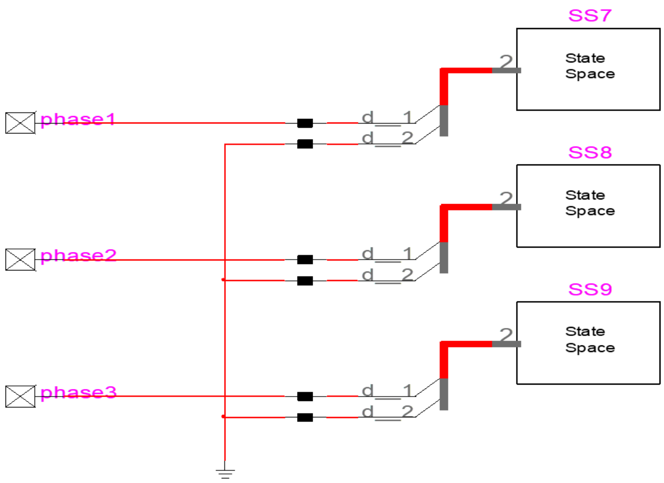

Figure 3.2: Black Box model of three-phase star-star transformer

3.1.2 Data Processing and Model Extraction

From frequency response data, the transformer's impedance and admittance are calculated as a function of frequency, which contains information about its dynamic response. The Vector Fitting (VF) algorithm is then used to fit a rational transfer function H(s) mathematically representing the transformer's frequency-dependent input-output response in the Laplace domain. VF method progressively determines the poles and zeros of the system and provides an incredibly good fit for data. Transfer functions derived above can be further converted into state-space or pole-zero representations that are directly usable in electromagnetic transient analysis packages such as EMTP. The methodology ensures that a model developed can mimic transformer behavior at a steady state and transients at a broad frequency spectrum.

3.1.3 Results and Applications

The outcome of this black-box modeling exercise is a set of six wide-band transformer models, one for each loading scenario, to investigate the transformer's behavior under switching transients, particularly those resulting from circuit breaker re-striking. These models have the transformer's frequency-dependent impedance and admittance properly modeled, which play important roles in deciding the behavior of the transformer when a circuit breaker fails to interrupt current properly and re-striking occurs. By simulating the effects of the re-striking phenomenon of breakers, measuring resulting high-frequency transient phenomena, and developing effective countermeasures by way of surge arresters and optimal breaker sequence of operation using these advanced simulations, system designers can improve the security of a system and reduce the possibility of transformer damage.

3.2

3.3 Underground Cable modeling-Wide band model

The Single Core Cable is chosen as a reference, and the datasheet is included in the appendix. WB (wideband) model of a single-core underground cable is developed for switching transients studies.

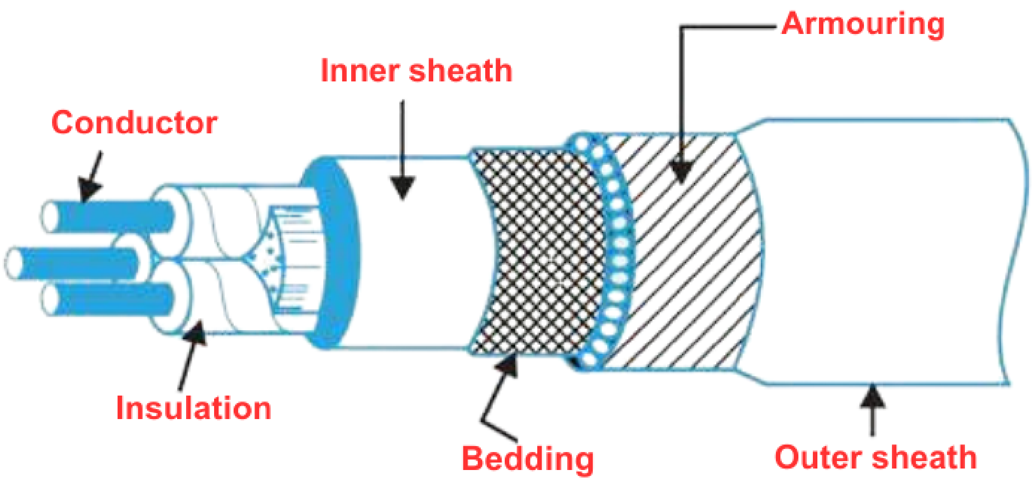

Figure 3.3: A single core Underground cable internal schematics

3.3.1 Wide-band Model

The wide band model of an underground cable is an advanced technique that portrays the behavior of the cable in a wide frequency range: from high-frequency transients to steady-state power frequencies. In this model, conductance, capacitance, inductance, and resistance are considered as frequency-dependent parameters due to changes caused by dielectric losses, proximity effects, and skin effects. It replaces the narrow band models, which assume that during its frequency range, the parameters are constant and supply an accurate, wide band model of the cable transient reaction when suddenly hit by fast-varying events such as switching operations or lightning strokes. Very relevant for transient analysis, in EMC studies, and insulation coordination, it makes a realistic simulation of tools such as EMTP possible. The wide band model allows detailed insight into the underground cables within complex power systems by accurate modeling over a broad range of frequencies.

3.3.2 Cable Data Geometry Input

In developing the cable data model to mimic the underground cable systems, one other step is to create the model of a cable from geometry. Users are allowed to choose their required depth level for the investigation with which different options such as the Wide-band model and the Frequency-Dependent Phase Domain (FDQ) model can be availed. These models perform well while representing electrical and electromagnetic behavior for cables over a wide range of frequencies. This procedure follows the subsequent steps using the reference model, which provides the starting point for the creation and evaluation of the cable configurations. Figure 3.5:wires are placed in

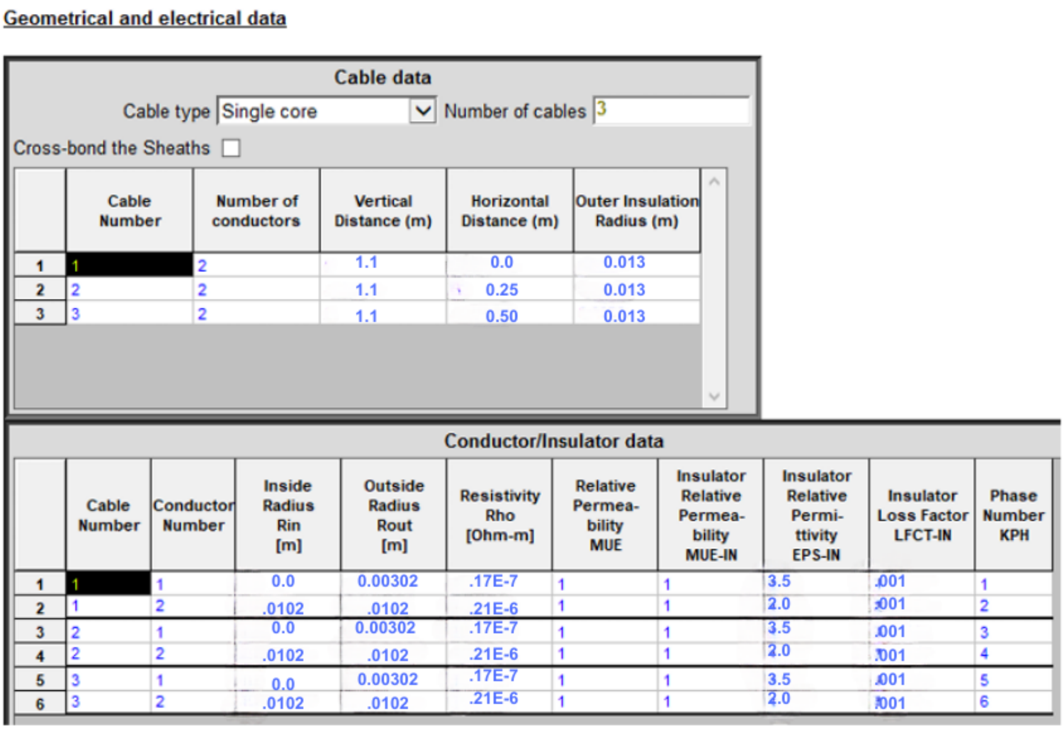

	Cable Number	Number of conductors	Vertical Distance (m)	Horizontal Distance (m)	Outer Insulation Radius (m)
1	1	2	1.1	0.0	0.013
2	2	2	1.1	0.25	0.013
3	3	2	1.1	0.50	0.013

	Cable Number	Conductor Number	Inside Radius Rin [m]	Outside Radius Rout [m]	Resistivity Rho [Ohm-m]	Relative Permea-bility MUE	Insulator Relative Permea-bility MUE-IN	Insulator Relative Permi-ttivity EPS-IN	Insulator Loss Factor LFCT-IN	Phase Number KPH
1	1	1	0.0	0.00302	.17E-7	1	1	3.5	.001	1
2	1	2	.0102	.0102	.21E-6	1	1	2.0	.001	2
3	2	1	0.0	0.00302	.17E-7	1	1	3.5	.001	3
4	2	2	.0102	.0102	.21E-6	1	1	2.0	.001	4
5	3	1	0.0	0.00302	.17E-7	1	1	3.5	.001	5
6	3	2	.0102	.0102	.21E-6	1	1	2.0	.001	6

Figure 3.4: Cable Data Model- Input Parameters

an intentional manner below the earth's surface at a designed depth Figure 3.6 Reference cable to verify the positive and zero-sequence impedance values for triangular cable configuration. A triangular layout is adopted because it is ideal due to the following reasons: the electromagnetic properties will be balanced: Due to a symmetrical distribution, and the operation of the cable will be performed with excellence.

The model has, as input, the positions of the three single-conductor cables in this triangular configuration. Each coaxial cable includes two conductors: an outer shield

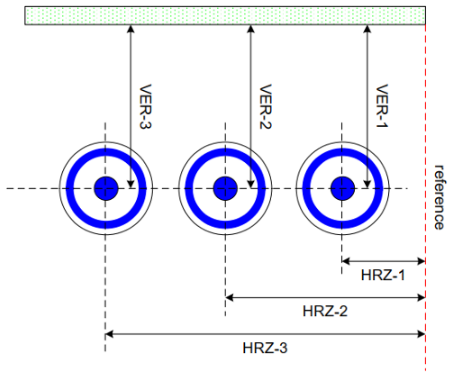

Figure 3.5: Cable Data Model- General Geometry Input [30]

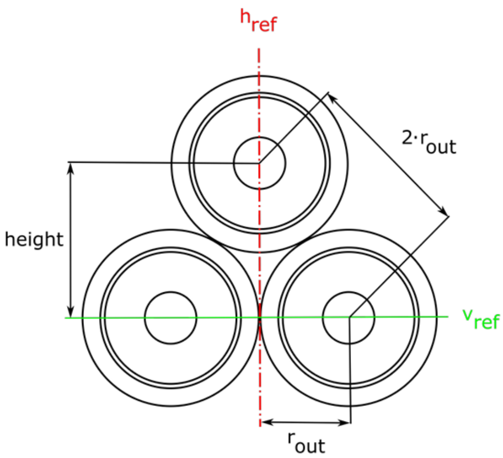

Figure 3.6: Triangle Position Cable [30]

and the central conductor at the core, separated by inner insulation. To achieve this triangular shape, the vertical and horizontal positions of the wires are measured from the outer radius with great accuracy. This is quite an exact geometric configuration, which is needed to simulate and analyze the electrical and transient behavior of the cable system in various situations. The table gives detailed data on single-core cable systems, including the conductor and insulator properties. The conductor uses copper with its standard resistivity and specified radii, and for insulation, it considers an 18 mm thick XPE layer with a permittivity of 3.5 and a loss factor of 0.001. Wrapping around this, additional layers include a semi-conductive water-blocking tape, an APL sheath, and an HDPE outer sheath with a graphite coat for durability and insulation. The shield is bulked by a bulking factor to accommodate manufacturing tolerances. The KPH number indicates how the conductors are connected. With KPH=0 merging conductors to ground, though here the shield is modeled as separately connected. This multi-layered design thus provides both electrical efficiency and structural integrity.

3.3.3 Wide-band model of underground cable simulated Characteristics in EMTP software environment

1. **Short-circuit impedance of the core conductor:**
   The wide band model of the 26/45kV ELAND underground cable, presented by the graph, shows the frequency-dependent short-circuit input impedance that is crucial in switching transient studies such as circuit breaker re-strikes. From the magnitude plot, we can observe that at low frequencies , the magnitude of the impedance is relatively low, approximately , due to the inductive character of the cable under power frequency operation. When the frequency is increased to 10^4

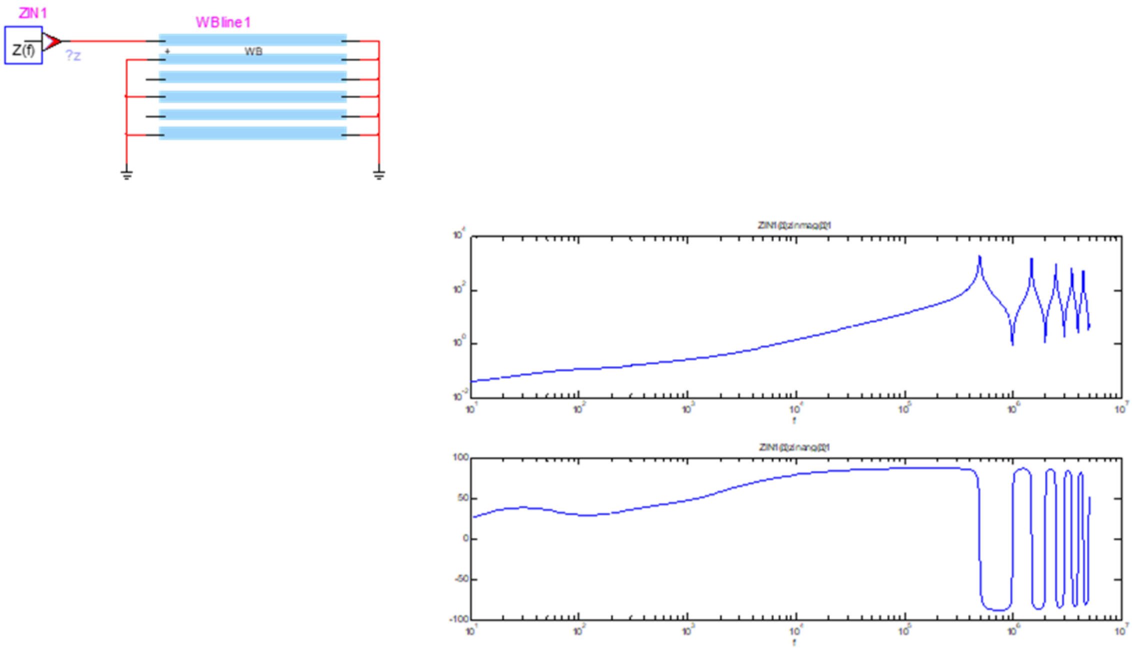

Figure 3.7: Short-circuit impedance of core conductor in wide band model of underground cable

Hz (10 kHz), the impedance value increases linearly . Of particular interest are the clear resonance peaks seen at 10^5 Hz (100 kHz), when impedance leaps to values of about 10^5 ohms (100 kΩ), indicating high over-voltage levels in rapid transients. In the phase plot, below low frequencies (below 1 kHz), the phase is around 0° to 20° with inductive behavior. At the resonant frequencies (around 100 kHz), the phase shifts rapidly towards -90° to -100° indicating a change towards capacitive dominance and high-resonant characteristics. These quantitative findings highlight the degree to which the cable's impedance response at different frequencies can influence the severity of switching transients, especially in re-striking conditions, justifying detailed transient analysis and mitigation techniques.

2. **Open-circuit impedance of core conductor:**
   Open-circuit input impedance of 26/45 kV ELAND cable has a high value of the order of $10^6\Omega$ at low frequency (close to 1 Hz), showing mainly a capacitive nature. With the increase in frequency to the order of 10 kHz, the impedance goes down gradually due to the growing effect of cable capacitance. Above 100 kHz, there are resonance effects and impedance oscillations between $1k\Omega$ and $100k\Omega$ are observed in the magnitude plot.

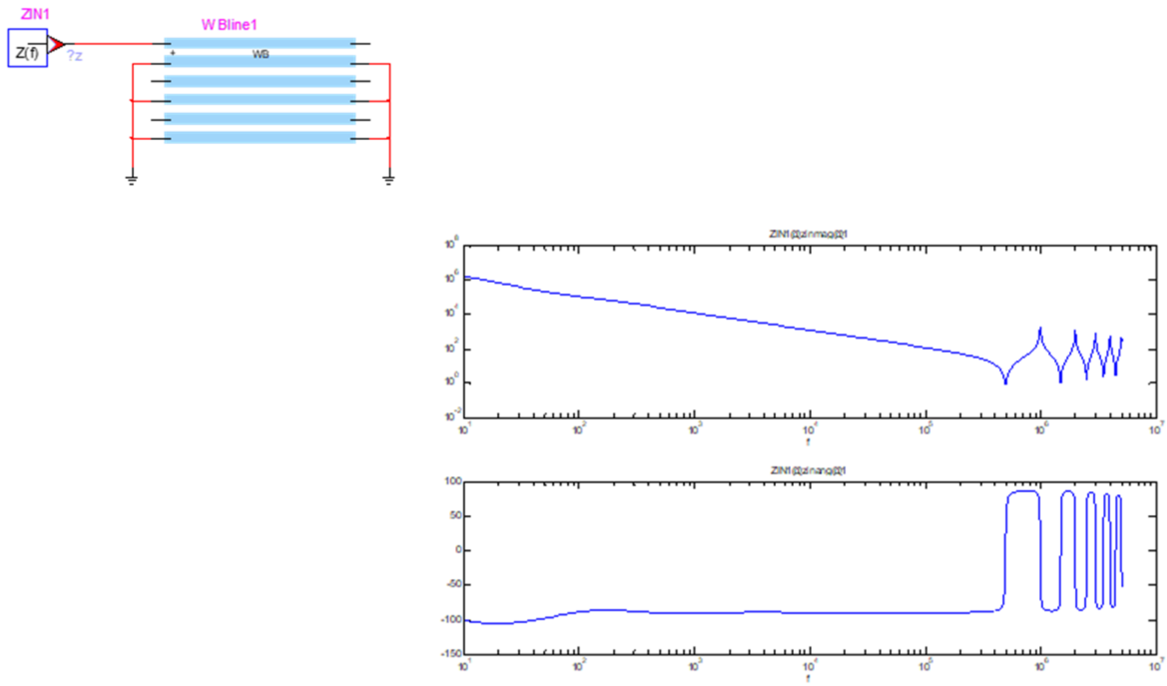

Figure 3.8: Open-circuit impedance of core conductor in wide band model of underground cable

The phase angle begins close to -90° at low frequencies, reaffirming capacitive dominance, but varies wildly above 1 MHz, denoting inductive and resonant interactions. All these characteristics are very important to transient over-voltage analysis since resonance peaks can reinforce switching surges in power networks.

3. **Short-circuit impedance of sheath conductor:** newline The sheath conductor input impedance of the wideband underground 26/45 kV cable is frequency

dependent. At low frequencies ($< 10Hz$), the magnitude of the impedance is quite low, around 1Ω, with predominantly resistive behavior. As the frequency increases up to 10 kHz, the impedance rises gradually to around 10Ω owing to the sheath inductance and proximity effects. Around 1 MHz, there are resonant

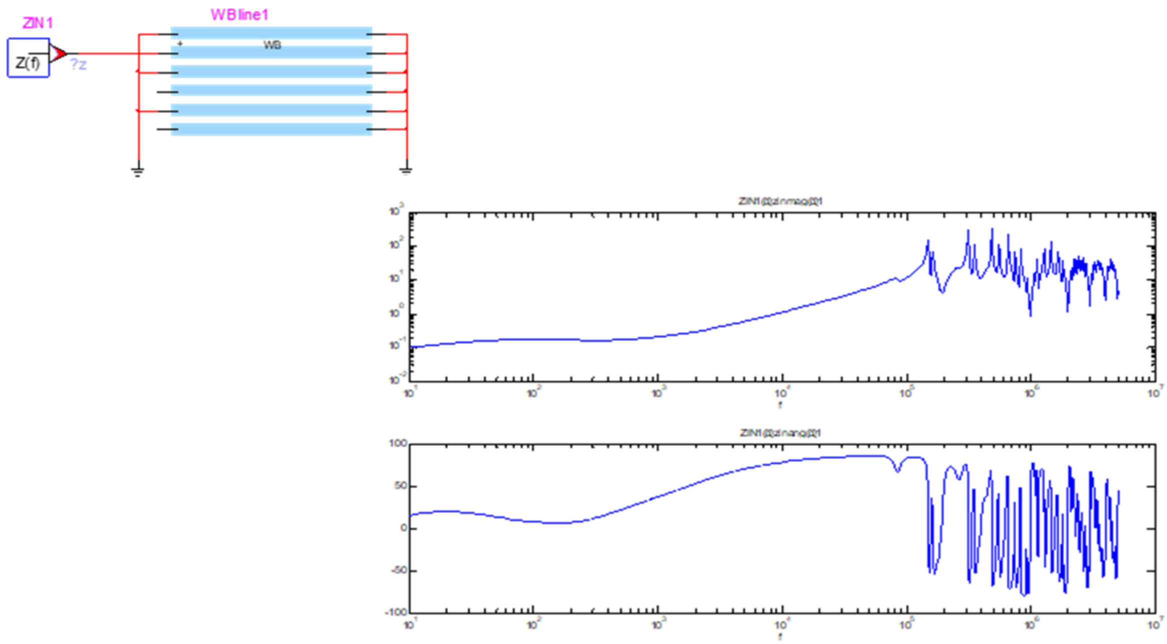

Figure 3.9: Short-circuit impedance of sheath conductor in wide band model of underground cable

effects with oscillations between 10Ω and 100Ω and high-frequency noise above 10 MHz due to wave propagation and eddy current losses. The phase response starts at around 0°, increases to 50-60° around 10 kHz, and fluctuates wildly above 1 MHz, indicating complex resonant interactions. These impedance characteristics are vital to transient analysis, grounding system design, and electromagnetic interference (EMI) analysis in underground power systems.

4. **Open-circuit impedance of sheath conductor:**
The open-circuit sheath conductor impedance, as one can determine from the graph, is of high initial impedance ($10^6\Omega$) at low frequencies, which is what one would expect with an open-circuited sheath that has no low-impedance current return path. Gradually reducing with increasing frequency down to 10Ω in the MHz frequency range, this demonstrates capacitive coupling between the sheath and phase conductors starting to dominate. At very high frequencies ($> 1MHz$), oscillation and resonance effects are observable as a consequence of the distributed behavior of the sheath and wave propagation effects over the cable length. The phase angle starts near -100° at low frequency, determining a predominantly capacitive behavior, and changes at increased frequencies due to resonance effects. This is typical of actual wide band underground cable models, though the practical losses will be suppressing some of the high-frequency.

5. **Voltage amplification factor on core conductor:**

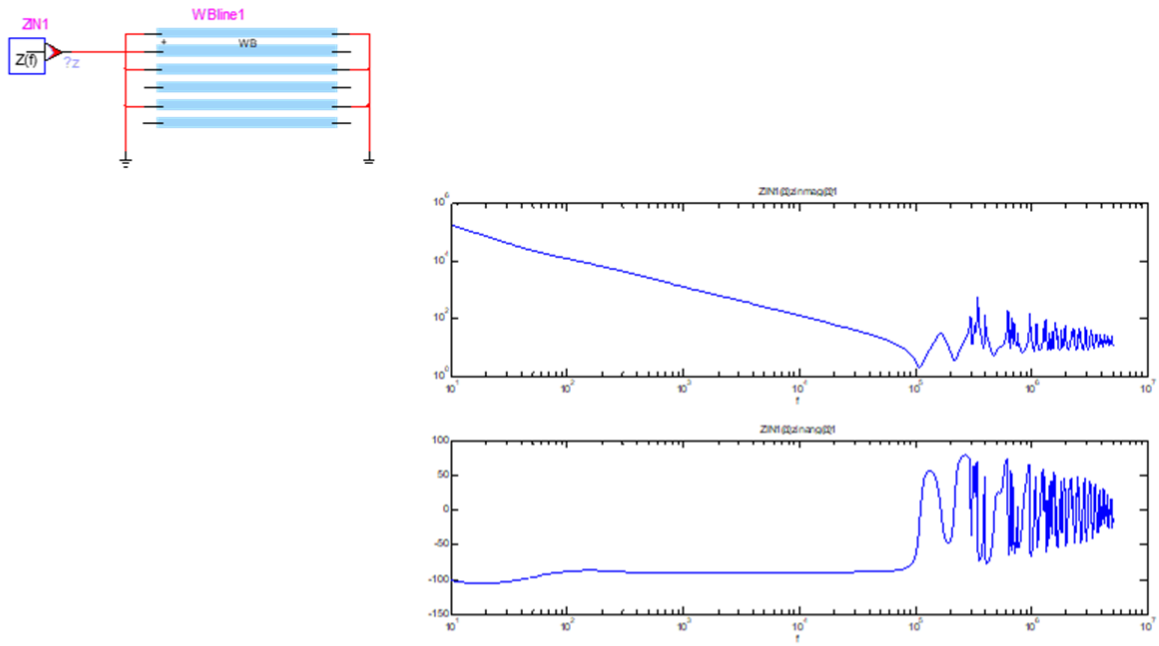

Figure 3.10: Open-circuit impedance of sheath conductor in wide band model of underground cable

The voltage amplification factor at the core conductor in the wide band model of a 26/45 kV cable is shown in the frequency domain. The magnitude plot (upper graph) is relatively low at lower frequencies but contains strong resonant peaks at higher frequencies ($> 10^5 Hz$ to $10^7 Hz$). The peaks indicate frequency-dependent resonances in which standing wave effects and reflections within the cable play a crucial role in leading to voltage amplification. The phase plot (lower plot) shows abrupt changes near the resonance points, characteristic of reactive impedance changes due to inductive and capacitive coupling within the cable. These results confirm real behavior, wherein resonance phenomena can lead to cable system over-voltages and greater severity under transient conditions. Proper grounding and damping techniques need to be invoked to avoid these amplifications in real applications.

6. **Voltage amplification factor of sheath conductor:**
The voltage amplification factor (VAF) of the 26/45 kV underground cable wide band model sheath conductor is particularly relevant under switching transients, whereby voltage steepness triggers resonant frequencies in the system. For low frequencies below $10^4 Hz$, the VAF is close to 1 and signifies minimal amplification. But during switching events, transient energy excites mid-to-high-frequency components, causing a rapid increase in sheath voltage at around 100 kHz ($10^5 Hz$), where the VAF is 10 (20 dB), signaling a huge amplification of transient over-voltages. Beyond 1 MHz ($10^6 Hz$), severe oscillations occur, with sheath voltage up to $200V$, corresponding to a VAF of 2, signaling persistent high-frequency ringing. These transient over-voltages are driven by wave reflections, frequency-dependent losses, and sheath-core interactions, hence the importance of proper surge mitigation techniques such as optimized grounding and damping circuits

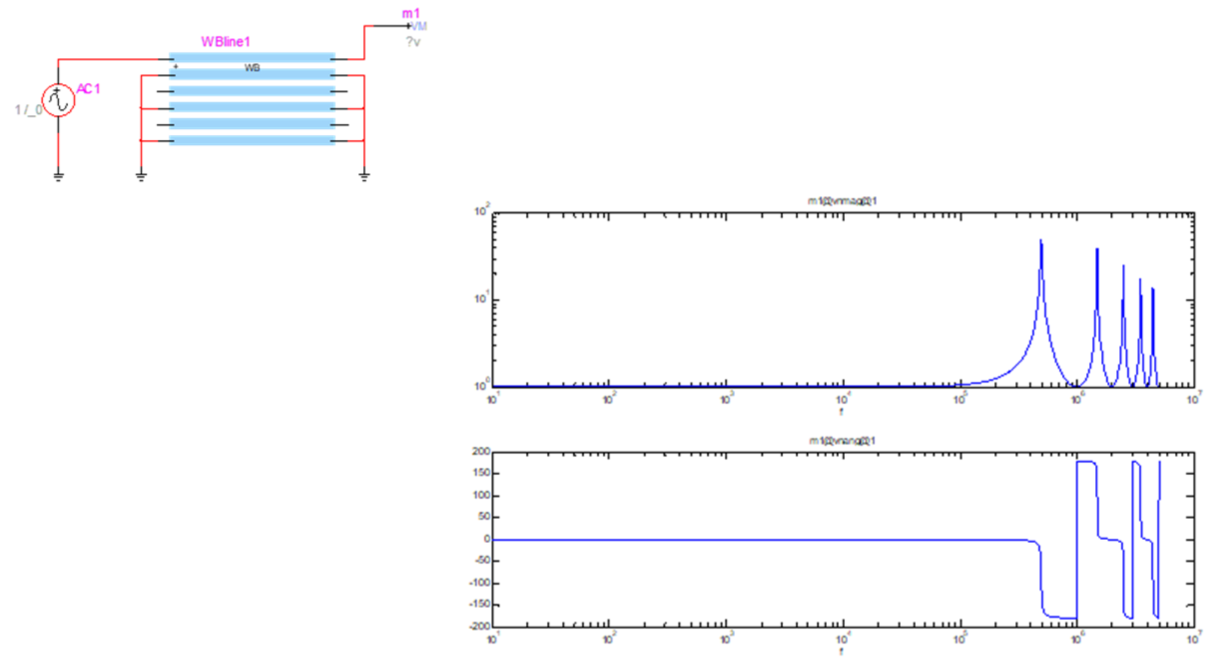

Figure 3.11: Voltage amplification factor on core conductor in wide band model of underground cable

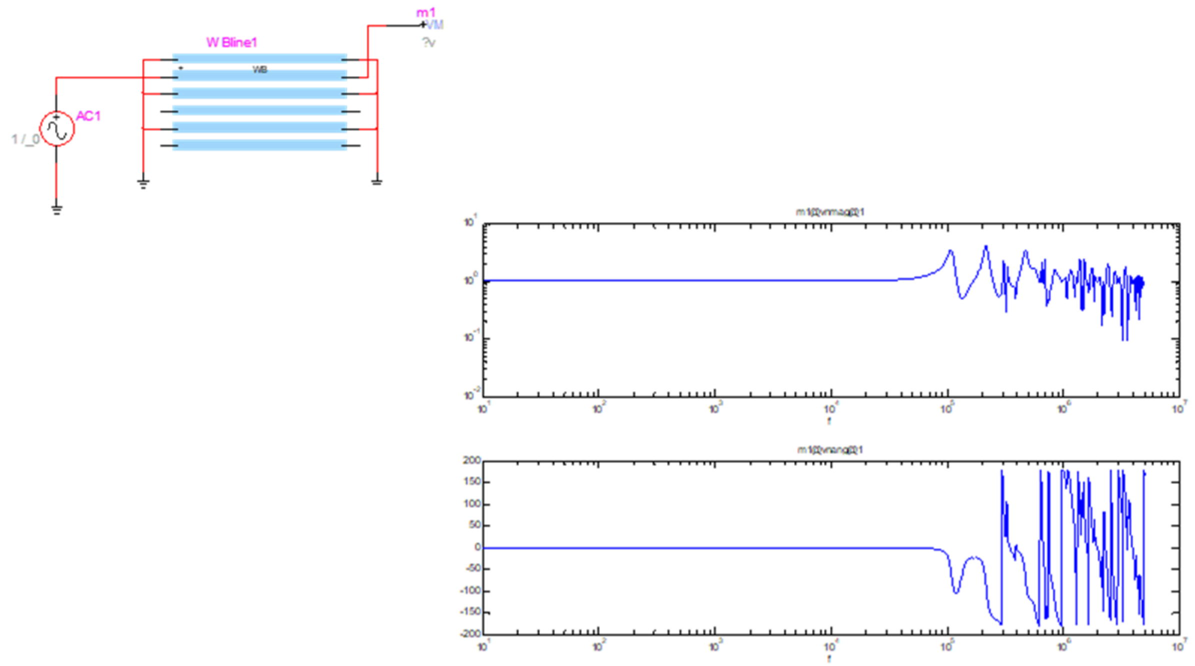

Figure 3.12: Voltage amplification factor of sheath conductor in wide band model of underground cable

to prevent sheath voltage amplification during the switching operation.

7. **Voltage transfer from core to the sheath on receiving end:**
The sheath-to-core voltage transfer at the receiving end of the 26/45 kV underground cable wide band model also has frequency-dependent properties with wide changes in amplitude for various frequency ranges. At low frequencies of up to $10^3 Hz$, the transfer function is comparatively low, with minimal voltage coupling. However, as the frequency is raised above $10^5 Hz$, the transfer function starts to increase and reaches a peak amplification at around 1 MHz ($10^6 Hz$), where there is a resonance-induced voltage transfer. The peak voltage level

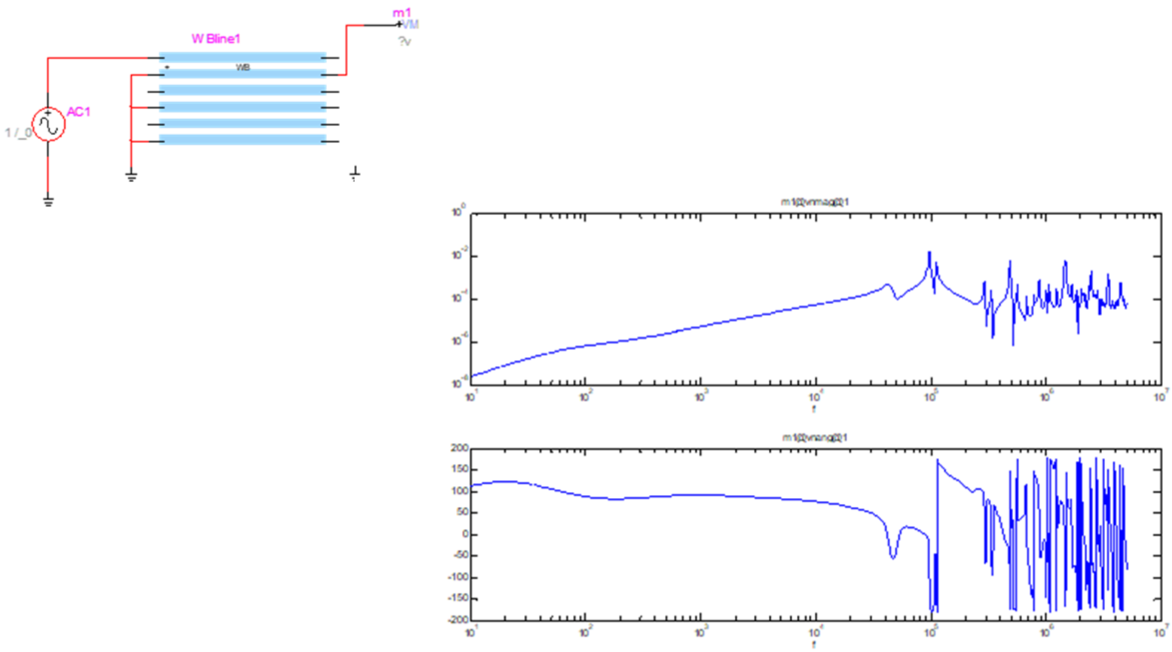

Figure 3.13: Voltage transfer from core to sheath on receiving end in wide band model of underground cable

within the sheath conductor at high frequencies is more than 150 V, showing that switching transients that contain high-frequency components can greatly influence sheath voltages. Above $10^6 Hz$, there exist intense oscillations with random voltage peaks due to wave reflections and resonance effects. This shows the importance of considering sheath voltage behavior when transient over-voltages in underground cables are dealt with, as improper grounding or insulation design can lead to excessive stress and potential failure of the cable system.

8. **Voltage transfer from core to sheath on sending end:**
The core-to-sheath voltage transfer at the sending end of the 26/45 kv underground cable wide band model is frequency-dependent and shares similar characteristics with those at the receiving end but with other features based on the source-side grounding and reflections. For low frequencies below $10^6 Hz$, the transfer function remains low, indicating strong insulation and minor coupling. With growing intensity above 10□ Hz, the transfer function rises slowly, peaking at about 1 MHz ($10^6 Hz$), where resonance leads to sheath voltage amplification.

The sheath voltage magnitude is estimated to be close to 150 V across most of the

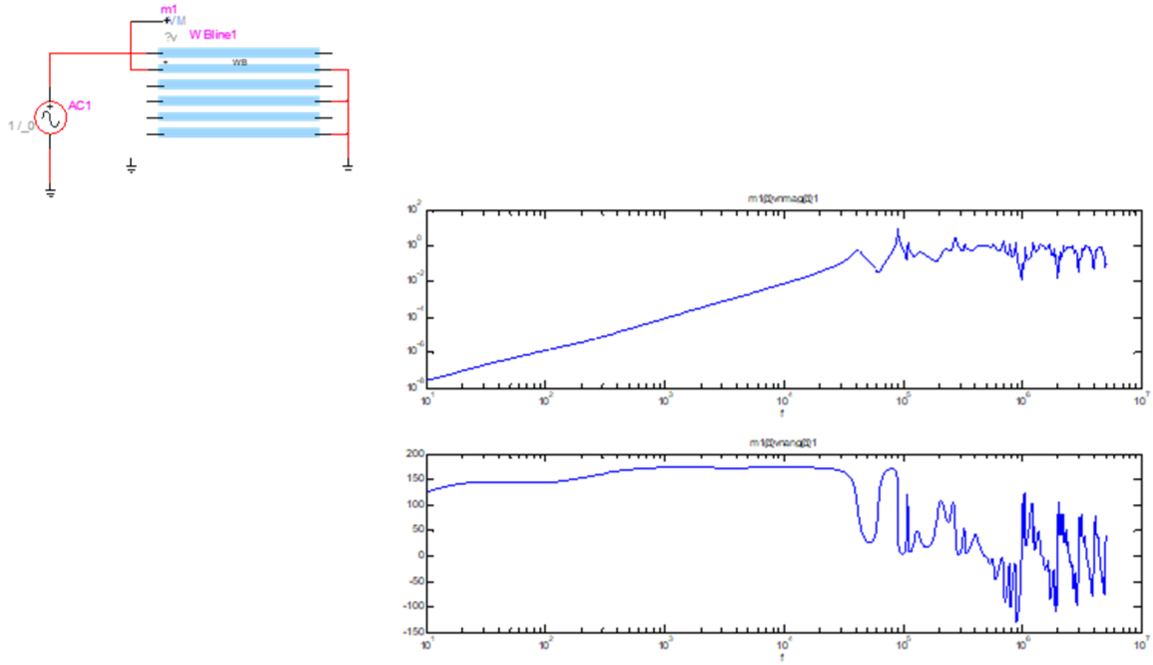

Figure 3.14: Voltage transfer from core to sheath on sending end in wide band model of underground cable

frequency range, but beyond $10^6 Hz$, spiky oscillations and voltage spikes arise due to wave propagation and high-frequency resonance effects. The increased coupling at high frequencies means that sharp wavefront switching transients can generate large sheath voltages at the sending end, which emphasizes the need for good grounding and mitigation techniques to reduce transient-induced sheath voltage stresses.

9. **Traveling-wave response on core conductor:**
   The traveling-wave response of the 26/45 kV wide band underground cable model presents a high-frequency oscillation of approximately 4 kHz with the first peak voltage of nearly 2.0 p.u. The wavefront arrives at the destination abruptly at 1.0 ms with a rapid propagation velocity of nearly $1.610m/s$, corresponding to the desired electromagnetic wave velocity in underground cables. The oscillations gradually decay as the signal hits 1.1 ms, reflecting frequency-dependent damping by the conductor and the dielectric loss The rise time of the wave is in the order of a few microseconds in magnitude with minimal initial dispersion but progressively weakening amplitude as the wave propagates along the cable. These attributes indicate the reason why the model accurately depicts transient overvoltage behavior which is crucial while analyzing switching surges and insulation stress in underground cable systems.

10. **Traveling wave response on sheath:**
    The sheath traveling-wave response of the 26/45 kV wide band underground cable has a distinct transient nature due to the core-sheath conductor coupling. The front peak voltage is approximately $1.6p.u.$ with a large induced transient in the

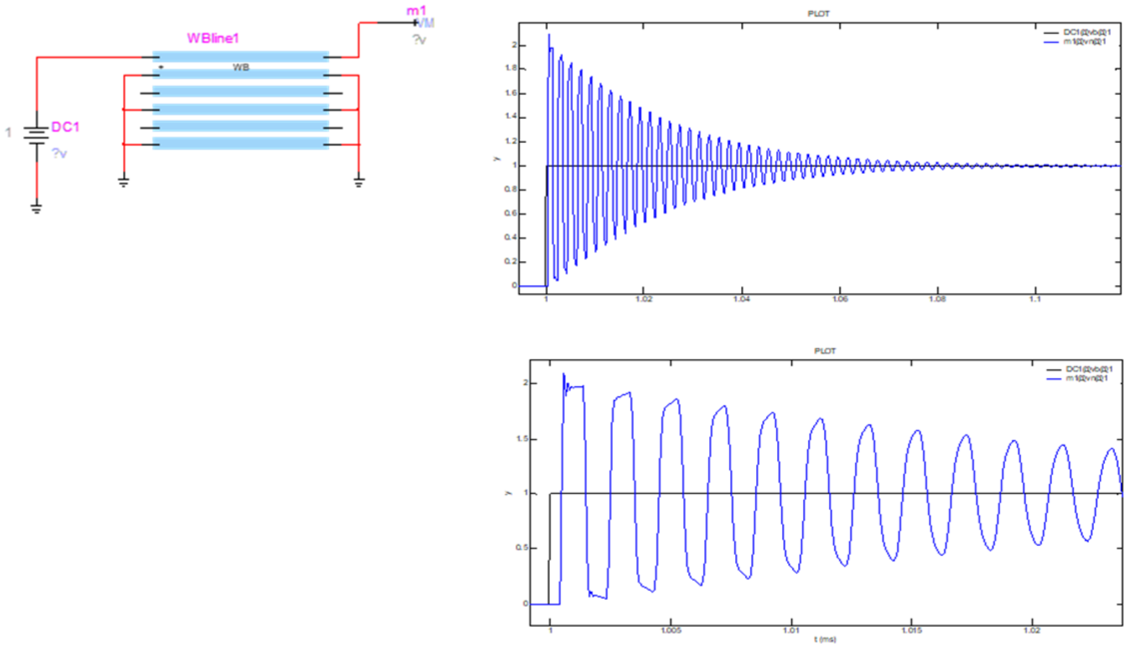

Figure 3.15: Traveling-wave response on core conductor in wide band model of underground cable

sheath. The wavefront rises steeply at around 1.0 ms with a propagation velocity near that of the core conductor ($1.610m/s$). However, compared with the core conductor response, the sheath experiences more irregular oscillations and larger damping, which is likely due to its lower inductance and additional resistive losses. The oscillations persist longer but exhibit significant attenuation after $1.07ms$, suggesting that the sheath absorbs and dissipates part of the transient energy. These characteristics set the reality that sheath voltage transients are controlled by electromagnetic coupling and grounding conditions and are, hence, needed for insulation coordination and over-voltage protection in underground cable systems.

3.4 Vacuum Circuit Breaker modeling-Black Box model

The functioning of a 36/40.5 kv vacuum circuit breaker is characterized by different parameters in its black-box model. The opening time and closing time of the breaker are denoted by t_{open} and t_{close}, respectively. They are parameters that determine how fast the circuit breaker can switch off the current or recover to normal mode after detecting a fault. While "t_{close}" controls how long the time will take for the breaker to close the circuit and restore it to service, reducing downtime, a smaller "t_{open}" indicates a fast fault-clearing time, which protects the system further. They play a vital role in coordinating relay protection schemes and preventing unnecessary stress on the electrical system.

The dielectric constants offered by the parameters A, B, C, and D are the insulating characteristics of the vacuum circuit breaker during switching. The dielectric constants symbolize the ability of the vacuum to withstand electrical stress and regain its insu-

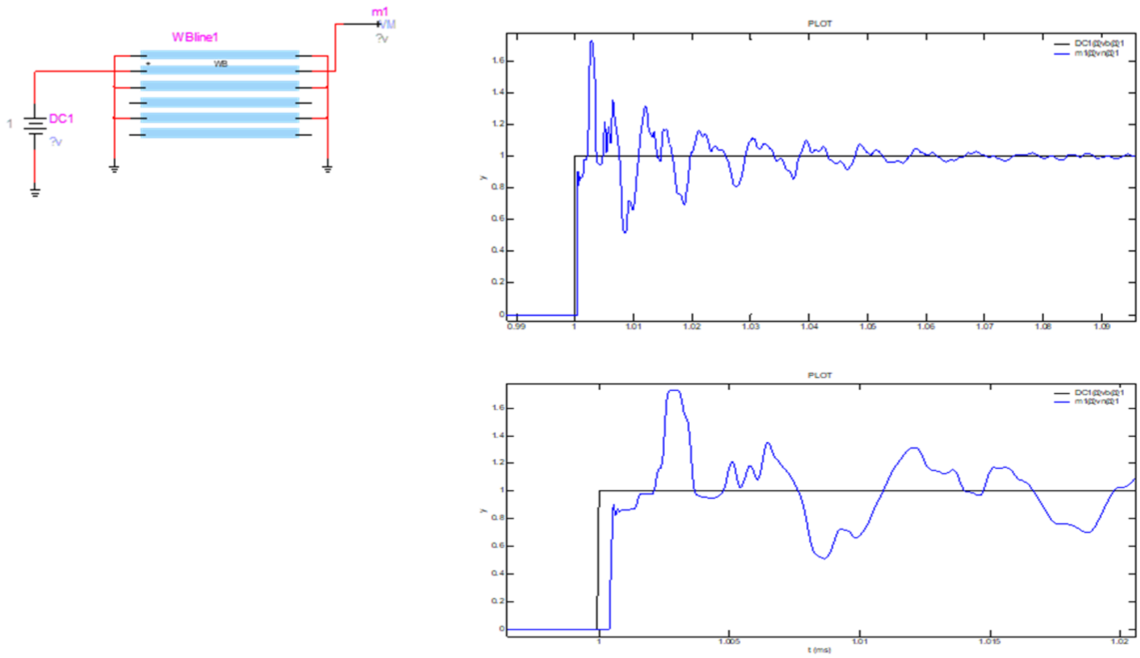

Figure 3.16: Traveling wave response on sheath in wide band model of underground cable

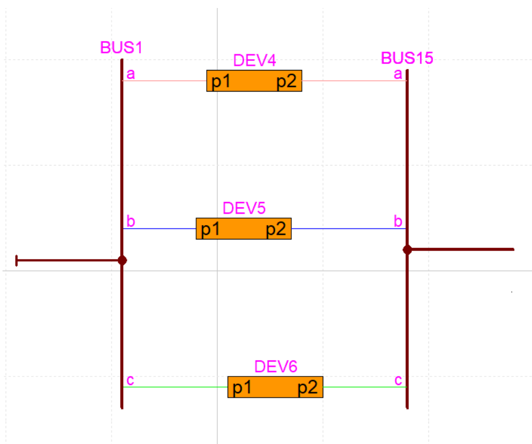

Figure 3.17: Black-Box Model of Vacuum Circuit Breaker realized in EMTP software environment

lating feature after an interruption in current. In the opening of the circuit breaker, the dielectric characteristics are required to avoid unwanted flashovers or re-strikes. The ability of the breaker to switch high voltage transients will depend on the value of A, B, C, and D, which also influence the breakdown voltage, contact gap insulation, and general dielectric performance.

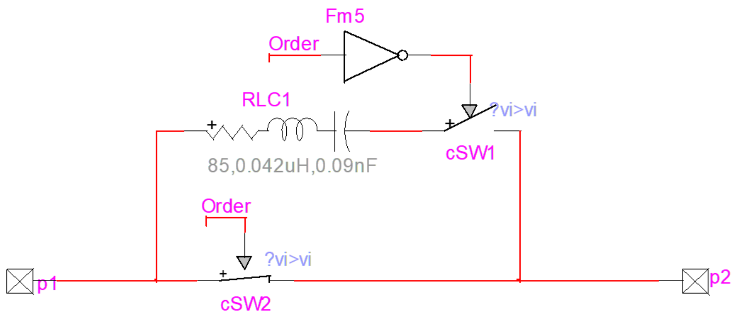

Figure 3.18: Vacuum Circuit Breaker switch realization circuit in EMTP software environment

In this study, the re-striking phenomena of switching transients occurring while the circuit breaker is trying to break the current flow but momentarily re-establishes the arc because of bad dielectric recovery is of specific concern to this research. Re-striking is a serious concern because it will lead to high over-voltages, damage to electrical equipment, and even system instability. One extremely significant parameter in the decision to restrike or not is the boundary between the transient recovery voltage (TRV) and the dielectric constants (A, B, C, and D). A circuit breaker can minimize re-striking and provide a safe disconnection process using proper dielectric strength and controlled switching characteristics.

In addition to this, re-striking is deemed in opposition to parasitic effects like R_{stray}, L_{stray}, and C_{stray}. Stray resistance (R_{stray}) is accountable for minimizing transient oscillation dampening by its capacity to control how rapidly the energy gets drained in the event of switching. Stray inductance (L_{stray}) voltage spikes and high-frequency oscillations are anticipated to cause re-strikes. Stray capacitance (C_{stray}) has an effect on dielectric recovery, the impact of which can have implications on the division of the voltage on contacts of a breaker. Vacuum circuit breakers can be designed by designers so that the frequency of re-striking is reduced and high reliability is ensured in high-voltage power systems with this knowledge of parameters and impact on switching transients.

Chapter 4

Switching Transient Analysis in a given Test System using Monte Carlo Simulation

4.1 Introduction

One of the statistical techniques for analyzing the impact of parameter changes on system behavior is **Monte Carlo analysis**.[popov2009trv] In this study, Monte Carlo simulations are utilized to examine the parameter variation in the vacuum circuit breaker during switching events on transient recovery voltage (TRV) and transformer voltage in a test system [popov2005transient] .Moreover, Transient recovery voltage (TRV) and transformer voltage response for different transformer loading are simulated by varying VCB parameters based on specified probability distributions.[31]

4.2 Vacuum Circuit breaker Parameters Variability and Probability Distributions

The following parameters, along with their respective probability distributions, are considered to define the uncertainty as well as variability in vacuum circuit breaker properties;

- **Opening Time** (T_{open});with uniform distribution between 5[ms] to 25[ms]
- **Chopping Current (I_{chop})**: with uniform distribution between 3[A] to 6[A]
- **Stray Inductance** (L_{stray}): with normal distribution with a mean of 0.05[uH] and std. of 15 %
- **Stray Capacitance (C_{stray})**:with normal distribution with a mean of 0.1[nF] and std. of 15 %
- **VCB Contact Withstand Voltage Speed (A)**: with normal distribution with a mean of 0.013[kV/us] and std. Of 15 %
- **VCB Contact Withstand Voltage Constant (B)**: with normal distribution with a mean of 0.69[kV] and std. Of 15 %
- **VCB HF Current Quenching Capability Rise (C)**: with normal distribution with a mean of 0.32[$A/\mu s^2$]

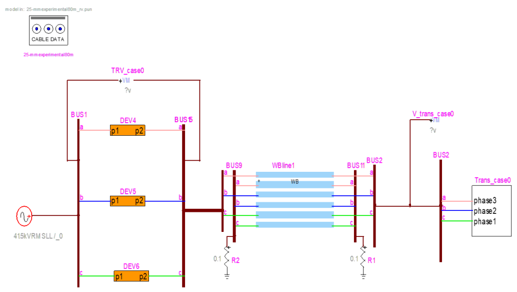

(a) Test System under No-Load condition

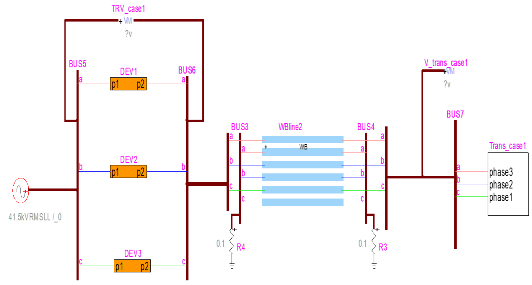

(b) Test System under Moderate-Load condition

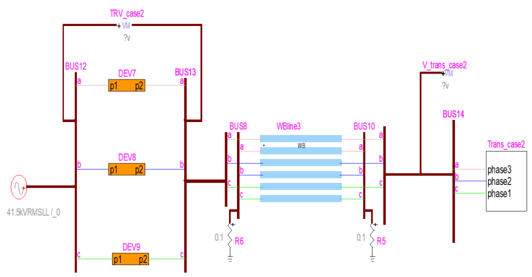

(c) Test System under High-Load condition

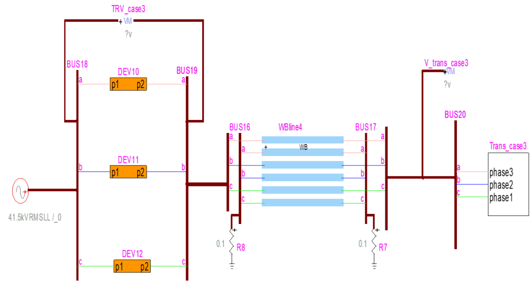

(d) Test System under Low-Capacitance condition

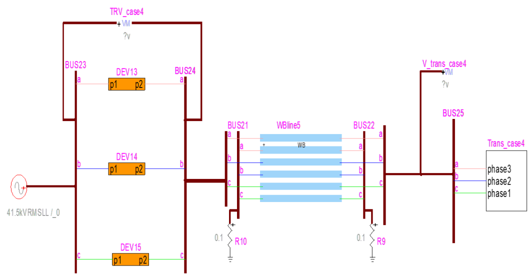

(e) Test System under High-Capacitance condition

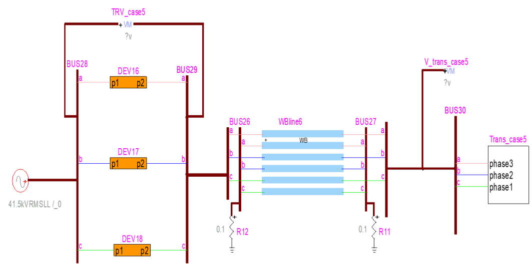

(f) Composite Impedance-Capacitance Scenario $(Z12\Omega \parallel Z3.3\mu F)$

Figure 4.1: Test System under various load conditions

- **VCB HF Current Quenching Capability Constant (D)**: with a mean of 375$[A/\mu s]$ and std. Of 75$[A/\mu s]$

4.3 Test System under various Load conditions

- **No-Load Scenario (Z_{nl})**: The reference case, representing the no-load state.

- **Moderate Load Scenario ($Z56\Omega$)**: A star-star transformer connected to a moderate resistive impedance of 56Ω.

- **High Load Scenario ($Z12\Omega$)**: A star-star transformer connected to a lower system impedance of 12Ω, representing high load conditions.

- **Low Capacitance Scenario ($Z0.047\mu F$)**: Includes a small capacitance of $0.047\mu F$ to model minimal capacitive effects.

- **High Capacitance Scenario ($Z3.3\mu F$)**: Introduces a significantly higher capacitance of $3.3\mu F$ to simulate dominant capacitive effects.

- **Composite Impedance-Capacitance Scenario ($Z12\Omega \parallel Z3.3\mu F$)**: A realistic mixed-condition scenario where a resistive load of 12Ω is in parallel with a high capacitance of $3.3\mu F$.

4.4 Simulation Results

4.4.1 Transient recovery voltage across different load scenarios in a test system during the synchronized opening of the vacuum circuit breaker

A comprehensive statistical analysis of transformer load conditions influencing Transient Recovery Voltage (TRV) behavior is carried out using Monte Carlo simulations. Six distinct load scenarios are considered: No Load (Z_{nl}), Moderate Load ($Z_{56\ \Omega}$), High Load ($Z_{12\ \Omega}$), Low Capacitance ($Z_{0.047\ \mu\mathrm{F}}$), High Capacitance ($Z_{3.3\ \mu\mathrm{F}}$), and a Composite Load ($Z_{12\ \Omega} \parallel Z_{3.3\ \mu\mathrm{F}}$). These cases highlight the critical role of system impedance and capacitance in shaping the transient response following the operation of a Vacuum Circuit Breaker. The simulation results reveal that TRV peak magnitudes and damping characteristics vary significantly across different loading conditions. This underscores the importance of accurate circuit breaker selection and tailored system design for reliable performance.

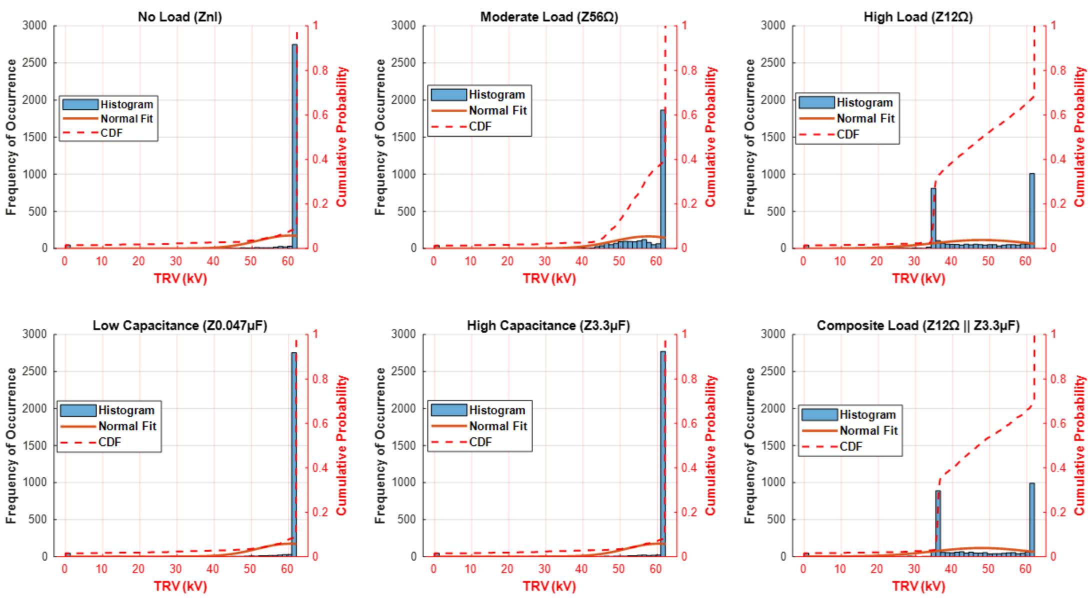

Figure 4.2: Transient recovery voltage across different load scenarios in a test system

1. **No-Load Case (Z_{nl}) – Severe Transient recovery voltage (TRV) Due to Weak Damping and Chopping Effects**
   The transformer undergoes low resistive damping on no load, which results in higher peak values of TRV. The Monte Carlo simulations show that TRV reaches

Scenarios	Mean (kV)	Max (kV)	Std Dev (kV)	2% Value (kV)
No Load (Z_{nl})	60.28	62.09	8.68	62.08
Moderate Load ($Z_{56\Omega}$)	57.42	62.07	9.28	62.06
High Load ($Z_{12\Omega}$)	47.81	62.06	13.27	62.04
Low Capacitance ($Z_{0.047\mu F}$)	60.30	62.10	8.70	62.08
High Capacitance ($Z_{3.3\mu F}$)	60.37	62.21	8.69	62.18
Composite Load ($Z_{12\Omega} \parallel Z_{3.3\mu F}$)	47.76	62.05	13.09	62.04

Table 4.1: Transient Recovery Voltage (TRV) Statistics

a mean of 60.28 kV, with a peak of 62.09 kV and a relatively small standard deviation of 8.68 kV. This is indicative of high TRV magnitude but relatively predictable behavior. Current chopping is one of the most serious issues in the no-load condition. Since the transformer carries a low load current, the vacuum circuit breaker interrupts at low current levels, increasing the possibility of chopping before a natural zero-crossing. The statistical results indicate that this leads to TRV waveforms with high slopes and rapid voltage build-up in most cases. In addition, re-ignition occurs in some of the Monte Carlo trials, where the chopped current oscillations cause the breaker gap to lose its dielectric strength temporarily, thereby leading to transient over-voltages.

2. **Moderate Load ($Z_{56\Omega}$) – Reduced Transient Recovery Voltage but Higher Variability**
   Monte Carlo simulation illustrates lower peak TRV values in case the transformer is loaded by a moderate resistive load of 56 Ω than if it is unloaded. At higher standard deviation of 9.28 kV, mean TRV is 57.42 kV and peak is 62.07 kV. This indicates that owing to the subtle interdependence of the load and transient oscillation, moderate loading imposes greater variability on TRV behavior. One of the key observations here is the presence of virtual current chopping. Under conditions in the external circuit in some simulations, the current drops abruptly before a natural zero, causing high-frequency oscillations that couple with TRV. This produces a broader spectrum of TRV rise times, as the increased standard deviation shows. However, because the resistive load provides some damping, the overall re-ignition probability is lower than in the no-load case.

3. **High Load ($Z_{12\Omega}$) – Stronger Damping but Higher Risk of Re-striking**
   During high-load scenario (12Ω), the Monte Carlo results have the smallest mean TRV (47.81 kV), with 62.06 kV being the highest and having the highest standard deviation (13.27 kV). It indicates a system that is damped with lower TRV, but due to the large standard deviation, the transients are less stable here. A key phenomenon in this case is re-striking. Since the breaker is interrupting a much larger current, arc energy is higher and there are several re-ignition events before final arc extinction in some simulations. Re-strikes produce several steep voltage spikes, stressing insulation systems and enhancing the likelihood of equipment failure unless proper surge suppression is used. In addition, since the high inductive current is being interrupted, voltage oscillations are worse during re-striking.

4. **Low Capacitance ($Z_{0.047\mu F}$) – Transient Recovery Voltage (TRV) Similar to No-Load but Slightly Higher Peak Values**
   With the low-capacitance scenario ($0.047\mu F$), Monte-Carlo simulation indicates TRV values almost equivalent to the no-load condition with a mean value of TRV equal to 60.30 kV and a peak value of 62.10 kV. The behavior remains largely unchanged because the added capacitance is minimal, meaning it does not significantly alter system transients.One small difference observed, however, is a minute increase in peak TRV values and a slight change in frequency of oscillation. Capacitance can, as a temporary charge storage device, generate higher initial peaks in TRV, though overall weak damping. Current chopping and reignition danger still continues to be high in this case, similar to the no-load case.

5. **High Capacitance ($Z_3.3\mu F$) – Increased Transient Recovery Voltage (TRV) Oscillations and Delayed TRV Effects.**
   The addition of high capacitance ($3.3\mu F$) significantly alters the Monte Carlo simulation results. The mean TRV is 60.37 kV, and the crest TRV reaches 62.21 kV, the highest among all cases. Oscillatory behavior in this case is robust, with TRV waveforms showing long-lasting high-frequency transients following current extinction.A dominant phenomenon in this case is delayed TRV effects. Due to the fact that the large capacitance stores charge, the TRV does not damped quickly after the arc is extinguished. Instead, post-arc oscillation persists, sometimes leading to voltage rise effects. The Monte Carlo analysis estimates that some cases exceed typical insulation design margins, i.e., high-capacitance circuits require special damping means such as surge arresters or snubber circuits.

6. **Composite Load ($Z_{12\Omega}$) $\parallel$ $Z_{3.3\mu F}$) – The Most Complex Transient Response**
   The composite impedance-capacitance scenario ($Z_{12\Omega}$) $\parallel$ $Z_{3.3\mu F}$) is the most challenging transient case in the Monte Carlo calculation. The mean TRV is 47.76 kV, and the peak TRV is 62.05 kV with a very high standard deviation of 13.09 kV. This indicates that the high inductive load with enormous capacitance results in damping oscillations as well as resonant oscillations, and thus, erratic behavior in TRV. Monte Carlo simulations prove that re-striking, virtual chopping, and delayed TRV effects all happen in different circumstances, making it the most difficult circumstance for insulation coordination. There are some waveforms with extreme post-arc oscillations, and others have high damping, depending on the particular conditions of interruption. The high standard deviation for TRV values supports the need for probabilistic analysis to predict worst-case conditions and take precautions accordingly with proper surge protection.

4.4.2 Voltage across transformer terminals in a 40 kV test system during the synchronized opening of the vacuum circuit breaker

A detailed statistical evaluation of the responses of transformer terminal voltages during the synchronized opening of vacuum circuit breakers was conducted for six load conditions employing Monte Carlo simulations. Such simulations analyze the randomness of voltage transients due to random variations in load impedance, breaker

Load Scenario	Mean TRV (kV)	Max TRV (kV)	Std Dev (kV)	Dominant Phenomena	Damping Effect
No Load (Z_{nl})	60.28	62.09	8.68	Current chopping, reignition, steep TRV rise	Weak (high TRV peaks)
Moderate Load ($Z_{56\Omega}$)	57.42	62.07	9.28	Virtual current chopping, moderate TRV steepness	Moderate
High Load ($Z_{12\Omega}$)	47.81	62.06	13.27	Restriking, multiple reignition events	Strongest (low TRV mean, high variability)
Low Capacitance ($Z_{0.047\mu F}$)	60.30	62.10	8.70	Similar to no-load, minor TRV frequency shift	Weak
High Capacitance ($Z_{3.3\mu F}$)	60.37	62.21	8.69	Delayed TRV effects, post-arc oscillations	Minimal (oscillatory TRV response)
Composite Load ($Z_{12\Omega} \parallel Z_{3.3\mu F}$)	47.76	62.05	13.09	Combination of restriking, virtual chopping, delayed TRV effects	Mixed (complex behavior, needs careful mitigation)

Table 4.2: Monte Carlo Simulation Results for Different Load Scenarios

parameters, and circuit topologies.

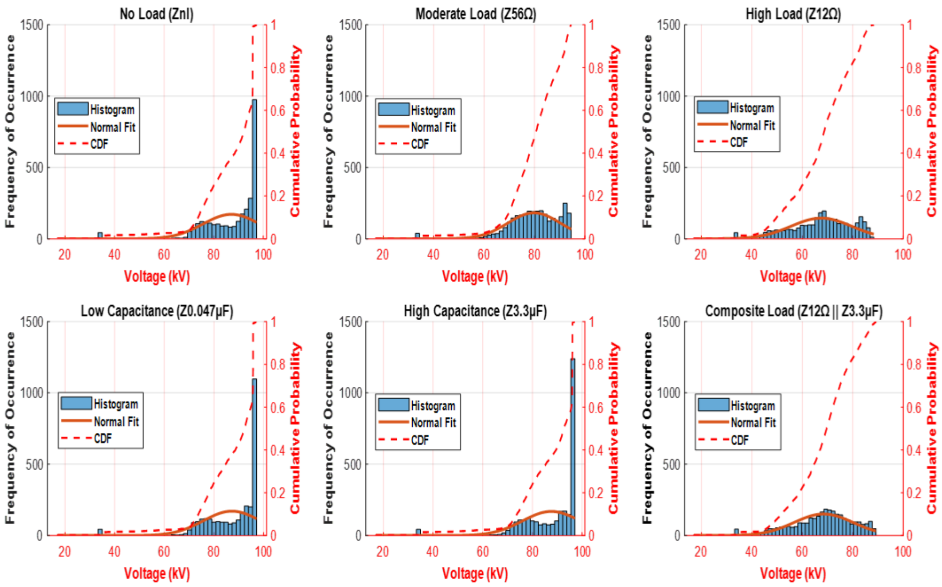

Figure 4.3: Transformer voltage across different load scenarios in a test system

1. **No Load (Z_{nl}) – High Peak transformer voltage and Weak Damping**
   At no load, the transformer experiences maximum mean voltage (87.12 kV) and peak voltage (97.30 kV), indicating zero energy dissipation through resistive elements. This is because the system is lightly damped, and the resonant oscillations may persist. Since there is no significant load to absorb energy, the voltage rises rapidly following circuit breaker action, especially after current chopping events. In addition, zero-crossing does not occur naturally, leading to overvoltages since the vacuum circuit breaker will interrupt very low currents too soon. The standard deviation is quite high (11.46 kV) since it reflects variability in transient voltage behavior due to the poor damping condition.

2. **Moderate Load ($Z_{56\Omega}$) – Improved Stability with Some Variability**
   The transformer's voltage characteristics with a moderate resistive load of 56Ω. The average voltage drops to 79.85 kV, and damping rises as a result of the resistive circuit's energy loss. As zero-crossing becomes more consistent, the

chances of current chopping occurring decrease. However, the transient behavior of the circuit can generate virtual chopping, which would provide minimal variability. Although the voltage transients are being damped, they can still be found to possess a very high amount of variance as depicted by peak voltage (94.54 kV) and standard deviation (10.42 kV). Damping effectiveness and system stress are being sacrificed here.

Scenarios	Mean (kV)	Max(kV)	Std Dev(kV)	2% Value(kV)
No Load (Z_{nl})	87.12	97.30	11.46	95.76
Moderate Load ($Z_{56\ \Omega}$)	79.85	94.54	10.42	93.76
High Load ($Z_{12\ \Omega}$)	67.54	88.34	12.05	85.75
Low Capacitance ($Z_{0.047\ \mu\text{F}}$)	87.23	97.18	11.48	95.79
High Capacitance ($Z_{3.3\ \mu\text{F}}$)	87.60	97.10	11.60	96.14
Composite Load ($Z_{12\ \Omega} \parallel Z_{3.3\ \mu\text{F}}$)	68.42	89.19	11.71	87.50

Table 4.3: Transformer Voltage Statistics (kV)

Load Scenario	Mean Voltage (kV)	Max Voltage (kV)	Std Dev (kV)	Dominant Phenomena	Voltage Behavior	Damping Nature
No Load (Z_{nl})	87.12	97.30	11.46	Voltage overshoot, resonance effects, absence of load current	High peak voltages, sharp rise at zero crossing	Very Weak (Minimal damping)
Moderate Load ($Z_{56\Omega}$)	79.85	94.54	10.42	Virtual chopping, improved zero-crossing behavior	Moderate voltage drop, controlled transient shape	Moderate (Resistive damping improves stability)
High Load ($Z_{12\Omega}$)	67.54	88.34	12.05	Restriking events, deep voltage sag, arc energy effects	Low voltage mean, wide oscillation spread	Strong (High resistive damping but erratic)
Low Capacitance ($Z_{0.047\mu F}$)	87.23	97.18	11.48	Similar to no-load, slight capacitive resonance	Near no-load voltage shape with small frequency shift	Weak (Capacitance too low to help damping)
High Capacitance ($Z_{3.3\mu F}$)	87.60	97.10	11.60	Post-arc oscillations, delayed zero crossing	Long-lasting oscillations, slow voltage decay	Very Weak (Capacitive rise dominates, minimal resistive damping)
Composite Load ($Z_{12\Omega} \parallel Z_{3.3\mu F}$)	68.42	89.19	11.71	Resonance between inductive load and high capacitance, complex interaction	Mixed response with large voltage swings and erratic damping	Mixed (Conflicting resistive
reactive damping sources)						

Table 4.4: Monte Carlo Simulation Results for Transformer Voltage Under Different Load Scenarios

Existing zero-crossing time greatly affects transformer voltage recovery. In the case of resistive loads (medium and high), natural zero-crossing allows for smoother interruption and limits voltage spikes. However, in no-load or low-capacitance conditions, zero-crossing may not occur simultaneously with breaker operation, and the sudden current interruption (chopping) may occur. This generates high-frequency components in the voltage waveform and leads to stress on transformer insulation. In the case of high-capacitance and composite, the stored energy may delay voltage reversal after interruption, resulting in a distorted and prolonged waveform with no definite zero-crossing characteristic.

Damping nature—resistive, reactive, or mixed—impacts significantly upon transformer voltage transient behavior. Light damping, such as in lightly loaded or over-capacitive systems, consists of large maximum voltages with prolonged oscillatory duration. Heavy damping, associated with high-load resistive loading, reduces voltage amplitudes but can feed instability by means of re-striking. Composite loads show that two concurrent, opposing mechanisms of damping will lead to dubious outcomes. These findings identify the requirements for specifically timed breaker, surge protective device, and damping components to facilitate the safe and effective operation of the transformer under different fault-clearing conditions.

Chapter 5

Conclusion and Future Work

5.1 Conclusion

This research work focused on the analysis of Transient Recovery Voltage (TRV) and transformer terminal voltages for a range of load conditions in a developed 40 kV test system. Monte Carlo simulations were performed in succession to obtain statistical details at various impedance conditions, including resistive, capacitive, and composite load arrangements. The purpose was to see how these electrical properties affect post-switching transients, especially the performance, and stress on circuit breakers and transformers in the course of switching operations.

The results of TRV presented a consistent peak value of voltage at around 62 kV for all the test cases. Despite variation of the mean values of TRV from 47.8 kV under high load conditions to 60.3 kV under low capacitance conditions — the 2% value was nearly constant. This illustrates that although the average breaker stress can vary with loading, the peak TRV in the extreme cases is more or less independent of the nature of the connected load. Interestingly, the highest standard deviation occurred in the high load and composite cases, reflecting a more random and unstable recovery process that needs to be considered in breaker insulation coordination.

Transformer terminal voltage response, however, was considerably more load-sensitive. At low-load and low-capacitance conditions, the system had high peak voltages over 97 kV with poor damping. These conditions caused resonant oscillations and rapid voltage rise near zero crossings, both of which impose stress on transformer insulation. Conversely, the addition of resistive elements — especially the 56Ω and 12Ω loads — reduced the voltage amplitude considerably and helped in producing a more tapered transient response.

The composite load condition, having a 12Ω resistor in parallel with a $3.3\mu F$ capacitor, showed the most complex transient response. Capacitive resonance, coupled with resistive damping, created voltage waveforms with large swings and chaotic rates of decay. This condition illustrates that composite load scenarios can potentially create confounding damping effects so that transformer response can't be predicted and protection equipment coordinated. The transformer voltage in this scenario had a standard deviation of 11.71 kV, which was widely deviated from the mean.

The most significant outcome of the analysis is the primary contribution damping has to the transformer voltage profile and TRV formation. Capacitive loads provided extended ringing with little attenuation, whereas resistive loads added extra damping and faster transient decay. The extended ringing and slow decay, especially in the large capacitance case, illustrate how crucial it is to consider capacitive elements in cable-connected systems. These conditions may result in over-stressing insulation or uncontrolled re-strikes of the breaker unless corrected.

The simulation results indicated in this research are in good correspondence with the observed behavior of actual high-voltage cable systems, especially for switching and energization operations. For example, high TRV under no-load and low-capacitance conditions correspond with field experience where re-strikes and insulation stress occur when underground cables are energized with no appreciable load current. These findings agree with known effects in which a lost damping — through lack of resistive load — allows high-frequency oscillations and steep voltage gradients, especially across transformer bushings and circuit breakers.

The simulations reproduce the maximum average TRV (60.28 kV), over 62 kV peaks, and high average transformer voltage (87.12 kV) for the no-load (Z_{nl}) scenario. This concurs with field situations in which the worst transients occur when weakly loaded or standby transformers are de-energized, typically during maintenance or at times of low demand. The vacuum circuit breaker switches small currents, leading to current chopping and high TRVs. Due to the lack of damping, there are high-frequency oscillations, which strain the insulation of the neighboring components. These effects are well reported in literature and utility field experience for lightly loaded feeders or backup transformers.

A resistive light load dampens the transformer and TRV peaks at no-load for the moderate load case (Z_{56}). Simulation results show a decreased transformer voltage mean (79.85 kV) and TRV means (57.42 kV), which is a phenomenon in actual systems where transient amplitudes are lowered by partial load disconnections. This is a representative feeder disconnection in suburban or mixed-load cases. In real grids, well-balanced loading increases damping and reduces the impact of current chopping, leading to softer wavefronts for voltage and reduced insulation stress. Your model is an accurate description of this attenuation, verifying the congruence of simulation with real switching events in medium-voltage systems.

The heavy load ($Z_{12\Omega}$) condition is the de-energization of heavy loads, such as industrial processes or electric vehicle charging stations. It is clearly shown that it yields the lowest TRV mean (47.81 kV) and lowest mean transformer voltage (67.54 kV), but the highest standard deviation (13.27 kV TRV) due to more current interruption dynamics. In practice, breaking high loads can cause arc instability in high-speed breakers like VCBs. While top voltages are minimized due to energy being lost in the load, the breaker can experience maximum dielectric stress through high dv/dt recovery—equivalent to your simulation's increased volatility and requiring proper breaker selection in commercial applications.

Finally, the capacitance-loaded ($Z_{0.047\mu F}$ and $Z_{3.3\mu F}$) and composite loading ($Z_{12\Omega} \parallel Z_{3.3\mu F}$) conditions are typical of cable-loaded installations such as underground substations, offshore platforms, or city grids with long cable runs. These conditions have higher transformer voltage peaks (up to 97.10 kV) and slightly higher TRV peaks, especially for high capacitance. Switching such networks in real life usually produces resonant oscillations and voltage amplification due to trapped charges and reflections, especially when switched at the wrong points on the waveform. These composite scenario simulation results—mean TRV of 47.76 kV and huge standard deviation of 13.09

kV—coincide with field experience, supporting the fact that the mixture of resistive and capacitive components generates the most unpredictable and dangerous transients, requiring intimate coordination between surge protection and insulation design.

5.1.1 Key Findings and Answer to the Research Questions

1. **How does the inclusion of a wide-band black-box transformer model influence the accuracy and fidelity of transient over-voltage prediction under various loading conditions in a developed test system during Vacuum circuit breaker switching?**
   The inclusion of a black-box transformer model with wide-band characteristics has a profound influence on the fidelity and accuracy of transient over-voltage prediction during vacuum circuit breaker (VCB) switching, as demonstrated in the thesis by 3000 probabilistic simulations across six loading conditions. The model, which is based on frequency-domain measurements on the HV side of a real dry-type Y–Y transformer, captures the frequency-dependent behavior necessary to simulate high-frequency transients accurately. Transient recovery voltage (TRV) statistics show that despite different loading conditions — from no-load to composite impedance–capacitance ($Z_{12\Omega} \parallel Z_{3.3\mu F}$) — the peak TRV is practically a constant (62 kV), but large differences for standard deviations and mean TRV values exist, particularly with low impedance and capacitance loads. For example, the composite load and high load cases exhibit the lowest mean TRV values (47.76 kV and 47.81 kV respectively) but the highest standard deviations (13.09 kV and 13.27 kV), indicating a higher spread in transient behavior due to the interaction of low resistance and capacitive impedance — a phenomenon only adequately modeled by wide-band modeling.

   Similarly, transformer voltage statistics favor the applicability of frequency-based modeling. For the no-load and high-capacitance scenarios, they remain so in mean and crest voltages (87kV and 97 kV, respectively). Nevertheless, both composite and high-load scenarios also exhibit a drastic reduction in mean voltage (68 kV) and peak values (88–89kV), also with greater variability. These findings substantiate that transient propagation and reflection behaviors are highly dependent on the scenario, being loaded by impedance of load as well as by internal resonance of the transformer. The wide-band model accurately represents these variations, showing how oscillations can be amplified by capacitive elements and how resistive loading damps them — nuances lost with a reduced transformer model. Thus, the use of a wide-band black-box model not only improves simulation precision but also provides a more realistic stress assessment of insulation, TRV withstand coordination and protection requirements for various real-world conditions.

2. **How can insights from scenario-based transient recovery voltage (TRV) behavior be leveraged to guide the optimal placement and sizing of overvoltage protection devices in complex power system configurations?**
   Implications of scenario-based TRV behavior may be vital to inform the optimal installation and rating of surge arresters in transformer–cable interaction networks, particularly probabilistic switching scenarios. Monte Carlo simulation of synchro-

nized de-energization revealed that different loading scenarios are associated with radically different transient over-voltage profiles, composite ($Z_{12\Omega} \parallel Z_{3.3\mu F}$) and high-load ($Z_{12\Omega}$) having the greatest standard deviations and wider TRV distributions. These conditions resulted in TRV peaks approaching or just above 62kV in the worst cases, which are of potential risk to the insulation coordination of the system. The variability and unpredictability noted—particularly because of randomness in VCB parameters such as chopping current and quenching ability—mean that surge arresters need to be sized not on average system behavior but on worst-case probabilistic extremes, e.g., the 2% TRV values from simulation results.

In addition, the location of the surge arresters is of utmost importance in the transformer and underground cable interaction network system because wave reflections and impedance mismatches at the transformer–cable interfaces may cause higher voltage stresses. The finding that high capacitance conditions ($Z_{3.3\mu F}$) showed higher damping and more stable TRV behavior suggests that surge arresters placed closer to cable terminations or transformer bushings where the oscillatory response is highest can better clamp over voltages. The research on the findings of the thesis concluded that arresters not only get installed at areas of highest risk but are also constructed to take into consideration infrequent but significant transient events. This offers greater protection for expensive equipment like dry-type transformers and lessens the risk of insulation failure upon the application of vacuum breakers.

3. **How do random variations in vacuum circuit breaker switching, analyzed using Monte Carlo simulations, affect the reliability of protection systems in medium-voltage networks ?**
The Monte Carlo approach, applied through 3000 probabilistic simulations, accurately simulates the inherent randomness of vacuum circuit breaker (VCB) switching behavior—e.g., variability of opening time, chopping current, and stray RLC parameters. The resulting statistical variation in transient recovery voltage (TRV) and transformer terminal voltages across six different loading conditions illustrates the high variability that can exist during de-energization. For instance, TRV's standard deviation is much higher under composite-load (13.09 kV) and high-load (13.27 kV) conditions compared to no-load (8.68 kV), thus, switching transients are more dispersed under mixed capacitive influences and low impedance. This variability can distort the expected transient profiles, thereby impacting how and when protection devices operate—introducing risks such as unintended relay trips or failure to isolate faults.

In real-world medium-voltage grids, protection coordination will typically be based on deterministic system performance. However, the Monte Carlo-based findings point out that neglecting stochastic variations in VCB performance can lead to underestimating worst-case transient conditions. Composite and capacitive loads, in particular, which generate larger peak voltages and slower decay rates, augment the stress on protective margins and insulation. Exclusion of provision for such random variations in their environments may lead to improper functioning of protection devices such as over-voltage relays, distance protection, or differential schemes. To ensure that the protection system would be reliable under a variety of operating conditions and unforeseen transient responses, Monte Carlo analysis is therefore incorporated into system planning and protection design.

5.2 Future Work and Recommendations

Future studies will further enhance probabilistic models with the inclusion of other uncertainties of the system, such as varied air conditions, aging characteristics of vacuum circuit breakers (VCBs), and transformer insulation aging. Future studies can incorporate machine learning techniques to better estimate worst-case transient conditions.

Adaptive switching methods in proportion to capacitance levels and loading conditions are the main recommendation to power utilities and system operators. This study illustrated that in no-load and low-capacitance conditions, transient over-voltages become more significant [32] . For minimizing transient values, regulated switching methods such as synchronized switching devices or pre-insertion resistors must be considered. To minimize the severity of transients and improve system stability, power system planners also have to take optimal placement of capacitance into account, e.g., optimal shunt capacitor placement.

Lastly, research in the future can be focused on hybrid mitigation strategies that utilize passive dampers along with active control techniques. DVRs and thyristor-controlled switches can be utilized to prevent insulation failure and equipment breakdown by providing real-time transient cancellation. Extension of the research to higher voltages (e.g., 33 kV or 69 kV) and other breaker technologies (e.g., SF_6 and vacuum hybrid breakers) will also provide an enhanced insight into transitory behaviors in other power networks. These developments will reduce the possibility of disastrous transient disturbances in modern electrical systems by developing more hardened and dependable switching systems.[33]

Chapter A

MATLAB Source Code

MONTE CARLO ANALYSIS OF SWITCHING TRANSIENTS IN VARIOUS LOAD CONDITIONS

```
clc; clear; close all;
% MONTE CARLO ANALAYSIS
% Load the .mat file
data = load('Data_probablistic.mat'); % Replace with actual filename

% Define scenarios and corresponding variable names
scenarios = {'Baseline', 'Moderate␣Load␣Ω(56)', 'High␣Load␣Ω(12)', ...
             'Low␣Capacitance␣(0.047F)', 'High␣Capacitance␣(3.3F)', 'Composite␣Ω(12␣||␣3.3F)
                 '};

trv_vars = { {'TRV_Scenario_NoLoada', 'TRV_Scenario_NoLoadb', 'TRV_Scenario_NoLoadc'}, ...
             {'TRV_Scenario_ModerateLoad_56ohma', 'TRV_Scenario_ModerateLoad_56ohmb', '
                 TRV_Scenario_ModerateLoad_56ohmc'}, ...
             {'TRV_Scenario_HighLoad_12ohma', 'TRV_Scenario_HighLoad_12ohmb', '
                 TRV_Scenario_HighLoad_12ohmc'}, ...
             {'TRVScenario_Lowcapacitancea', 'TRVScenario_Lowcapacitanceb', '
                 TRVScenario_Lowcapacitancec'}, ...
             {'TRVScenario_Highcapacitancea', 'TRVScenario_Highcapacitanceb', '
                 TRVScenario_Highcapacitancec'}, ...
             {'TRVScenario_resicapaa', 'TRVScenario_resicapab', 'TRVScenario_resicapac'}};

trans_vars = { {'Vtrans_Scenario_NoLoada', 'Vtrans_Scenario_NoLoadb', '
    Vtrans_Scenario_NoLoadc'}, ...
               {'V_trans_ModerateLoad_56ohma', 'V_trans_ModerateLoad_56ohmb', '
                   V_trans_ModerateLoad_56ohmc'}, ...
               {'V_trans_Scenario_HighLoad_12ohma', 'V_trans_Scenario_HighLoad_12ohmb', '
                   V_trans_Scenario_HighLoad_12ohmc'}, ...
               {'V_trans_Scenario_Lowcapacitancea', 'V_trans_Scenario_Lowcapacitanceb', '
                   V_trans_Scenario_Lowcapacitancec'}, ...
               {'V_trans_Scenariohighcapacitancea', 'V_trans_Scenariohighcapacitanceb', '
                   V_trans_Scenariohighcapacitancec'}, ...
               {'V_trans_Scenario_resicapaa', 'V_trans_Scenario_resicapab', '
                   V_trans_Scenario_resicapac'}};

% Initialize results
results_TRV = [];
results_Trans = [];

% Compute statistics for TRV
for s = 1:length(trv_vars)
    combined_trv = [];
    for i = 1:length(trv_vars{s})
        combined_trv = [combined_trv; data.(trv_vars{s}{i}) / 1000]; % Convert V to kV
    end
    % Compute statistical metrics
    trv_mean = mean(combined_trv);
    trv_std = std(combined_trv);
    trv_max = max(combined_trv);
    trv_2perc = prctile(combined_trv, 98);
    results_TRV = [results_TRV; trv_mean, trv_std, trv_max, trv_2perc];
end
```

```

% Compute statistics for Transformer Voltage
for s = 1:length(trans_vars)
    combined_trans = [];
    for i = 1:length(trans_vars{s})
        combined_trans = [combined_trans; data.(trans_vars{s}{i}) / 1000]; % Convert V to kV
    end
    % Compute statistical metrics
    trans_mean = mean(combined_trans);
    trans_std = std(combined_trans);
    trans_max = max(combined_trans);
    trans_2perc = prctile(combined_trans, 98);
    results_Trans = [results_Trans; trans_mean, trans_std, trans_max, trans_2perc];
end

% Create and display tables
TRV_Table = array2table(results_TRV, 'VariableNames', {'Mean_kV', 'StdDev_kV', 'Max_kV', '98
    Perc_kV'}, 'RowNames', scenarios);
Trans_Table = array2table(results_Trans, 'VariableNames', {'Mean_kV', 'StdDev_kV', 'Max_kV',
    '98Perc_kV'}, 'RowNames', scenarios);

disp('------␣TRV␣Statistics␣------');
disp(TRV_Table);

disp('------␣Transformer␣Voltage␣Statistics␣------');
disp(Trans_Table);
```

VECTOR FITTING FOR DEVELOPMENT OF BLACK BOX MODEL OF STAR-STAR TRANSFORMER ,660kVA

```

clc
close all
clear all

addpath('functions')
addpath('temp')

% filename = 'ZP_Transformer.txt';
% [bigY, s] = Zextract(filename);

files = load('T_case5.mat');
s = files.s;
bigY = files.bigY;


%===============================================
%=            POLE-RESIDUE FITTING              =
%===============================================
opts.N=20 ;%            %Order of approximation.
opts.poletype='logcmplx'; %Mix of linearly spaced and logarithmically spaced poles
opts.Niter1=7;    %Number of iterations for fitting sum of elements (fast!) --> Improved
    initial poles
opts.Niter2=4;    %Number of iterations for matrix fitting
opts.asymp=2;      %Fitting includes D
opts.logx=1;       %=1 --> Plotting is done using linear abscissa axis
opts.weightparam = 2;
poles=[];
[SER,rmserr,bigYfit,opts2]=VFdriver(bigY,s,poles,opts); %Creating state-space model and pole-
    residue model


%===============================================
%=            Passivity Enforcement             =
%===============================================
clear opts;
opts.plot.s_pass=2*pi*1i*linspace(0,2e5,1001).';
opts.plot.ylim=[0.95 1.05]; opts.Niter_out=20;
opts.Niter_in=5;
opts.parametertype='Y';
```

```
opts.outputlevel=0; %Min. output to screen
opts.cmplx_ss = 0;
[SER,bigYfit_passive,opts3]=RPdriver(SER,s,opts);
SER.A = full(SER.A);
SER.B = full(SER.B);


%=================================================================
%= Comparing original model with perturbed model in fitting band =
%=================================================================
figure(11),
Nc=length(SER.D);
for row=1:Nc
  for col=row:Nc
    dum1=squeeze(bigYfit(row,col,:));
    dum2=squeeze(bigYfit_passive(row,col,:));
    h1=semilogy(s/(2*pi*1i),abs(dum1),'b'); hold on
    h2=semilogy(s/(2*pi*1i),abs(dum2),'r--');
    h3=semilogy(s/(2*pi*1i),abs(dum2-dum1),'g-');
  end
end
hold off
set(gca, 'XScale', 'log', 'YScale', 'log')
xlabel('Frequency [Hz]'); ylabel('Scattering matrix');
legend([h1 h2 h3],'Original model','Perturbed model','Deviation');
```

Chapter B

Appendix

GEAFOL
Cast-Resin Transformers

Rated power	Rated primary voltage tapping ± 2 x 2.5 %	Rated secondary voltage (no-load)	Insulation level HV (AC/LI)	Insulation level LV (AC/LI)	Impedance voltage at rated current	No-load losses	Load losses at 120 °C	Noise level	Order No.	Total weight	Length	Width	Height
S_r	U_r HV	U_r LV			u_{zr}	P_o	P_{k120}	L_{WA}		approx.	a 2)	b 2)	h 2)
kVA	kV	kV	kV	kV	%	W	W	dB		kg	mm	mm	mm
400	10	0.4	28/75	3/–	4	1150	4400	68	**4GB5644-3CA05-0AA2**	1290	1370	820	1230
	10	0.4	28/75	3/–	4	880	4400	60	**4GB5644-3GA05-0AA2**	1500	1390	820	1330
	10	0.4	28/75	3/–	6	1000	4900	68	**4GB5644-3DA05-0AA2**	1230	1400	820	1215
	10	0.4	28/75	3/–	6	800	4900	60	**4GB5644-3HA05-0AA2**	1390	1430	820	1230
	20	0.4	50/95	3/–	4	1450	3800	68	**4GB5664-3CA05-0AA2**	1470	1460	830	1285
	20	0.4	50/95	3/–	4	1100	3800	60	**4GB5664-3GA05-0AA2**	1710	1520	835	1305
	20	0.4	50/95	3/–	6	1200	4300	68	**4GB5664-3DA05-0AA2**	1380	1490	835	1260
	20	0.4	50/95	3/–	6	940	4300	60	**4GB5664-3HA05-0AA2**	1460	1500	840	1260
	20	0.4	50/125	3/–	6	1200	4700	68	**4GB5667-3DA05-0AA2**	1530	1540	845	1310
	30	0.4	70/145	3/–	6	1650	5500	69	**4GB5675-3DA05-0AA2**	1590	1560	925	1500
(500)1)	10	0.4	28/75	3/–	4	1300	5900	69	**4GB5744-3CA05-0AA0**	1490	1410	820	1315
	10	0.4	28/75	3/–	4	1000	5300	61	**4GB5744-3GA05-0AA0**	1620	1420	820	1340
	10	0.4	28/75	3/–	6	1200	6400	69	**4GB5744-3DA05-0AA0**	1420	1450	820	1245
	10	0.4	28/75	3/–	6	950	6400	61	**4GB5744-3HA05-0AA0**	1540	1490	820	1265
	20	0.4	50/95	3/–	4	1700	4900	69	**4GB5764-3CA05-0AA0**	1550	1460	840	1365
	20	0.4	50/95	3/–	4	1300	4900	61	**4GB5764-3GA05-0AA0**	1700	1490	845	1370
	20	0.4	50/95	3/–	6	1400	5100	69	**4GB5764-3DA05-0AA0**	1500	1530	855	1275
	20	0.4	50/95	3/–	6	1100	5100	61	**4GB5764-3HA05-0AA0**	1670	1560	860	1290
	20	0.4	50/125	3/–	6	1400	6300	69	**4GB5767-3DA05-0AA0**	1610	1540	855	1355
	30	0.4	70/145	3/–	6	1900	6000	70	**4GB5775-3DA05-0AA0**	1810	1560	925	1615
	30	0.4	70/170	3/–	6	2600	6200	79	**4GB5780-3DA05-0AA0**	2110	1710	1005	1590
630	10	0.4	28/75	3/–	4	1500	7300	70	**4GB5844-3CA05-0AA0**	1670	1410	820	1485
	10	0.4	28/75	3/–	4	1150	7300	62	**4GB5844-3GA05-0AA0**	1840	1440	820	1485
	10	0.4	28/75	3/–	6	1370	7500	70	**4GB5844-3DA05-0AA0**	1710	1520	830	1305
	10	0.4	28/75	3/–	6	1100	7500	62	**4GB5844-3HA05-0AA0**	1850	1560	835	1330
	20	0.4	50/95	3/–	4	2000	6900	70	**4GB5864-3CA05-0AA0**	1790	1470	840	1530
	20	0.4	50/95	3/–	4	1600	6900	62	**4GB5864-3GA05-0AA0**	1930	1520	845	1565
	20	0.4	50/95	3/–	6	1650	6800	70	**4GB5864-3DA05-0AA0**	1750	1560	860	1365
	20	0.4	50/95	3/–	6	1250	6800	62	**4GB5864-3HA05-0AA0**	1900	1600	865	1385
	20	0.4	50/125	3/–	6	1650	7000	70	**4GB5867-3DA05-0AA0**	1830	1590	865	1395
	30	0.4	70/145	3/–	6	2200	6600	71	**4GB5875-3DA05-0AA0**	2090	1620	940	1640
(800)1)	10	0.4	28/75	3/–	4	1800	7800	72	**4GB5944-3CA05-0AA0**	1970	1500	820	1535
	10	0.4	28/75	3/–	4	1400	7800	64	**4GB5944-3GA05-0AA0**	2210	1530	825	1535
	10	0.4	28/75	3/–	6	1700	8300	72	**4GB5944-3DA05-0AA0**	2020	1590	840	1395
	10	0.4	28/75	3/–	6	1300	8300	64	**4GB5944-3HA05-0AA0**	2230	1620	845	1395
	20	0.4	50/95	3/–	4	2400	8500	72	**4GB5964-3CA05-0AA0**	2020	1550	850	1595
	20	0.4	50/95	3/–	4	1900	8500	64	**4GB5964-3GA05-0AA0**	2220	1570	855	1595
	20	0.4	50/95	3/–	6	1900	8200	72	**4GB5964-3DA05-0AA0**	2020	1610	870	1435
	20	0.4	50/95	3/–	6	1500	8200	64	**4GB5964-3HA05-0AA0**	2220	1650	875	1455
	20	0.4	50/125	3/–	6	1900	9400	72	**4GB5967-3DA05-0AA0**	2160	1660	880	1485
	30	0.4	70/145	3/–	6	2650	7900	72	**4GB5975-3DA05-0AA0**	2620	1740	965	1695

1) Ratings in brackets are not

2) Dimension drawing: page 14

Connection System

Practice-oriented options for connection of the high-voltage and the low-voltage side are a distinguishing feature of the flexible connection philosophy of GEAFOL transformers.

Connection of the high-voltage side

In the standard design, the HV connection of the transformer is at the top coil connection, connection at the bottom is available as an option (Fig. 1). Screwed connection tubes are used for the delta connection. The transformer connection is made at the end of the connection tubes.

Connection of the high-voltage side using plug-type connectors

Connection of the HV side by using outside cone plug-type bushings is possible (see Fig. 2)

High-voltage tappings

The HV tappings allow matching to local network conditions. In deenergized state, the desired tapping can be selected by means of connection straps and screwed connections.

Connection of the low-voltage side

In the standard design, the LV connection of the transformer is also at the top; connection at the bottom is available as an option (Fig. 3).

If intermediate expansion links are employed, the LV side connection is protected against mechanical stress and transmission of structure-borne noise is drastically reduced.

Connection of earthing and short-circuiting devices

Either straight or angled spherical/earthing points, of diameter 20 mm or 25 mm, can be mounted at the connection tubes of the HV side and at the LV side at the conductor terminal face.

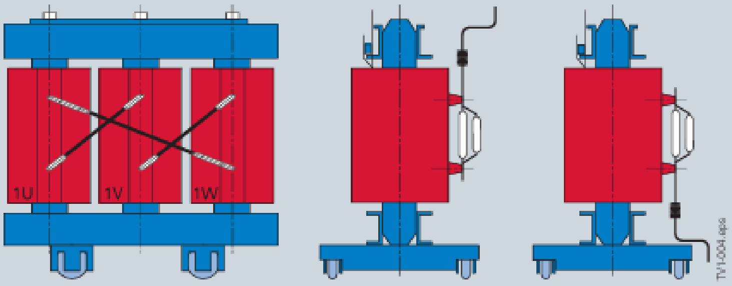

Fig. **1**
Variable connection possibilities,
e.g. at the delta-connected HV side

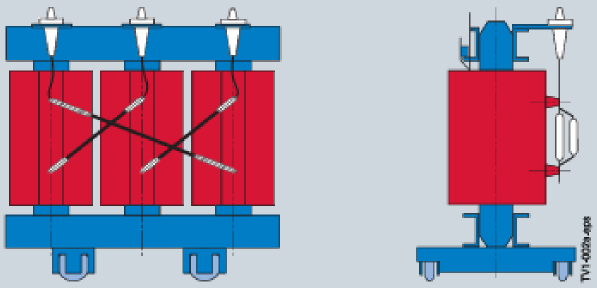

Fig. **2**
Plug-type HV connectors

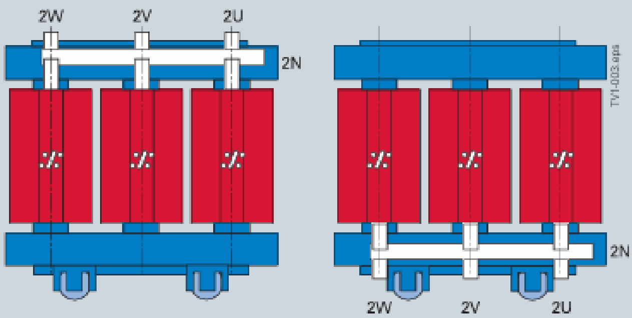

Fig. **3**
LV connection system on GEAFOL transformers
left Fig.: Phase and neutral connection at top
right Fig.: Phase and neutral connection at bottom

ELAND® CABLES

Click here for more information:
elandcables.com | A2XS(FL)2Y MDPE High Voltage 26/45 (52) kV Cable

A2XS(FL)2Y MDPE High Voltage 26/45 (52) kV Cable

Eland Product Group: H9F

APPLICATION

High Voltage cables for distribution networks; also for connection to generation units and plant and process connection. For installation in ground, in water outdoors, indoors and in cable ducts for power stations, industry and distribution networks. The water blocking tape avoids water propagation inside the cable.

CHARACTERISTICS

Voltage Rating Uo/U
26/45 (52) kV

CONSTRUCTION

Conductor
Aluminium conductor (optional watertightness – WTC)

Conductor Screen
Semi-conductive screen extruded on the phase conductor

Insulation
XLPE (Cross-linked Polyethylene)

Insulation Screen
Semi-conductive screen extruded on insulation

Wrapping
Semi-conductive water swelling tape

Metallic Screen
Copper wires and equalising tape

Wrapping
Semi-conductive water swelling tape

Tape
Longitudinally applied aluminium tape coated with PE copolymer

Sheath
MDPE (Medium Density Polyethylene)

Optional – semi-conductive layer

Sheath Colour
● Black

STANDARDS

IEC 60840

THE CABLE LAB®

AN ISO/IEC 17025 AND IECEE CBTL ACCREDITED FACILITY

Our world-class testing facility assures the quality and compliance of this cable through a continuous and rigorous testing regime.

ISO/IEC 17025 Accredited Testing Laboratory | IECEE CBTL Accredited Testing Laboratory

SUSTAINABILITY COMMITMENT

We are on a journey to Net Zero.

We've committed to near-term emissions reductions and a net-zero target with the Science Based Targets initiative and we're a signatory to the United Nations Global Compact Sustainable Development Goals.

Learn more about embodied carbon and our carbon emissions reduction actions, our comprehensive recycling services, and wider ESG activities for sustainable operations at: www.elandcables.com/company/about-us/esg-sustainability

SCIENCE BASED TARGETS | BUSINESS AMBITION FOR 1.5°C

REGULATORY COMPLIANCE

This cable meets the requirements of the RoHS Directive 2011/65/EU. RoHS compliance has been tested and confirmed by The Cable Lab® as meeting the requirements of the BSI RoHS Trusted Kitemark™.

bsi. RoHS Trusted KITEMARK™ | RoHS

Click here for more information:
elandcables.com | A2XS(FL)2Y MDPE High Voltage 26/45 (52) kV Cable

DIMENSIONS

ELAND PART NO.	NO. OF CORES	NOMINAL CROSS SECTIONAL AREA mm²	NOMINAL DIAMETER OF CONDUCTOR mm	INSULATION mm		METALLIC SCREEN		NOMINAL OUTER DIAMETER OF CABLE mm	NOMINAL WEIGHT kg/km	MAXIMUM PULLING FORCE mm	MINIMUM BENDING RADIUS m
				Nominal thickness	Nominal diamter over	Nominal cross section mm²	Nominal diameter over mm				
H9F45KV010095	1	95RM	11.3	9.0	30.5	35	34.3	41	1690	3.3	1.0
H9F45KV010120	1	120RM	12.5	9.0	31.7	35	35.5	42	1810	4.2	1.1
H9F45KV010150	1	150RM	14.1	9.0	33.3	35	37.1	43	1940	5.3	1.1
H9F45KV010185	1	185RM	15.8	9.0	35.0	35	38.8	45	2110	6.5	1.1
H9F45KV010240	1	240RM	17.9	9.0	37.1	35	40.9	47	2350	8.4	1.2
H9F45KV010300	1	300RM	20.0	9.0	39.2	35	43.0	49	2590	10.5	1.2
H9F45KV010400	1	400RM	22.9	9.0	42.5	35	46.7	53	3040	14.0	1.3
H9F45KV010500	1	500RM	25.7	9.0	45.3	35	49.5	56	3470	17.5	1.4
H9F45KV010630	1	630RM	29.3	9.0	49.1	35	53.3	60	4030	22.1	1.5
H9F45KV010800	1	800RM	33.0	9.0	52.8	35	57.0	64	4650	28.0	1.6
H9F45KV011000	1	1000RM	38.0	9.0	58.2	35	62.8	71	5570	35.0	1.8
H9F45KV011200	1	1200RM	42.5	9.0	62.7	50	67.3	75	6560	42.0	1.9
H9F45KV011200R	1	1200RMS	43.0	9.0	65.2	50	69.8	78	6840	42.0	2.0
H9F45KV011400	1	1400RMS	45.1	9.0	67.3	50	71.9	80	7490	49.0	2.0
H9F45KV011600	1	1600RMS	48.5	9.0	70.7	50	75.3	84	8270	56.0	2.1
H9F45KV011800	1	1800RMS	52.7	9.0	74.9	50	79.5	88	9170	63.0	2.2
H9F45KV012000	1	2000RMS	54.5	9.0	76.7	50	81.3	90	9760	70.0	2.3
H9F45KV012500	1	2500RMS	59.0	9.0	82.2	50	87.2	97	11270	87.5	2.4
H9F45KV013000	1	3000RMS	67.0	9.0	90.2	50	95.2	105	13690	100.0	2.6

ELECTRICAL DATA

De – Cable diameter

Cables in flat formation, the distance between the cable axes = 2 × De

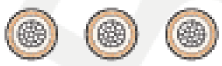

Cables in trefoil formation, the distance between the cable axes = De

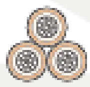

ELECTRICAL CHARACTERISTICS

NOMINAL CROSS SECTIONAL AREA mm²	NOMINAL RESISTANCE OF CONDUCTOR 90 °C Ω/km	ELECTRICAL FIELD STRESS kV/mm		CAPACITANCE µF/km	ZERO REACTANCE Ω/km	INDUCTANCE Ω/km	
		Conductor screen	Insulation			Flat formation	Trefoil formation
95RM	0.4110	4.70	1.95	0.150	0.087	0.200	0.145
120RM	0.3247	4.55	2.00	0.160	0.083	0.195	0.140
150RM	0.2645	4.40	2.05	0.175	0.078	0.190	0.135
185RM	0.2108	4.25	2.10	0.185	0.074	0.185	0.130
240RM	0.1610	4.15	2.15	0.205	0.069	0.180	0.125
300RM	0.1291	4.00	2.20	0.220	0.065	0.180	0.120
400RM	0.1009	3.90	2.25	0.245	0.062	0.175	0.115
500RM	0.0792	3.80	2.30	0.265	0.058	0.170	0.110
630RM	0.0622	3.70	2.35	0.295	0.055	0.165	0.105
800RM	0.0498	3.60	2.40	0.320	0.052	0.160	0.105

Click here for more information:
elandcables.com | A2XS(FL)2Y MDPE High Voltage 26/45 (52) kV Cable

NOMINAL CROSS SECTIONAL AREA mm²	NOMINAL RESISTANCE OF CONDUCTOR 90 °C Ω/km	ELECTRICAL FIELD STRESS kV/mm		CAPACITANCE µF/km	ZERO REACTANCE Ω/km	INDUCTANCE Ω/km	
		Conductor screen	Insulation			Flat formation	Trefoil formation
1000RM	0.0408	3.50	2.45	0.360	0.049	0.160	0.100
1200RM	0.0359	3.45	2.45	0.395	0.046	0.155	0.095
1200RMS	0.0319	3.45	2.50	0.415	0.048	0.155	0.095
1400RMS	0.0275	3.40	2.50	0.430	0.047	0.155	0.095
1600RMS	0.0242	3.40	2.55	0.455	0.045	0.155	0.095
1800RMS	0.0216	3.35	2.55	0.485	0.043	0.150	0.095
2000RMS	0.0195	3.35	2.55	0.500	0.042	0.150	0.095
2500RMS	0.0168	3.30	2.60	0.540	0.042	0.150	0.090
3000RMS	0.0130	3.25	2.60	0.600	0.039	0.150	0.090

CURRENT RATING FOR SINGLE-CORE CABLES – AMPERES

NOMINAL CROSS SECTIONAL AREA mm²	FLAT FORMATION				TREFOIL FORMATION				FLAT FORMATION				TREFOIL FORMATION			
	CONFIGURATIONS															
	SPP; CB		BOTH-ENDS		SPP; CB		BOTH-ENDS		SPP; CB		BOTH-ENDS		SPP; CB		BOTH-ENDS	
	CABLES IN EARTH								CABLES IN AIR							
	65°C	90°C	65°C	90°C	65°C	90°C	65°C	90°C	65°C	90°C	65°C	90°C	65°C	90°C	65°C	90°C
95RM	220	265	215	260	210	255	210	250	235	320	230	315	205	280	205	275
120RM	250	300	245	290	240	285	235	285	275	370	265	360	235	320	235	320
150RM	280	340	270	325	270	320	265	320	310	420	300	405	265	365	265	360
185RM	320	385	305	365	305	365	300	360	360	485	340	460	305	415	305	415
240RM	370	445	345	420	355	425	345	420	420	570	395	540	360	490	355	485
300RM	420	505	385	465	400	480	390	470	485	655	445	610	415	565	405	555
400RM	485	580	430	525	455	550	445	535	565	765	505	695	480	660	470	645
500RM	555	665	455	580	520	625	505	610	660	890	575	790	560	765	545	745
630RM	635	765	520	640	595	715	570	690	770	1045	645	895	650	890	625	865
800RM	725	870	560	695	670	810	635	770	890	1210	715	1000	745	1025	715	985
1000RM	815	980	600	745	750	905	700	850	1025	1395	790	1110	850	1175	805	1115
1200RM	885	1070	595	745	805	975	730	895	1135	1545	810	1145	935	1290	865	1205
1200RMS	930	1115	610	760	870	1040	780	950	1185	1605	830	1170	1010	1375	925	1275
1400RMS	1005	1210	630	790	940	1130	830	1015	1300	1755	870	1235	1100	1505	995	1380
1600RMS	1085	1300	650	815	1005	1210	875	1070	1415	1910	910	1290	1195	1635	1065	1480
1800RMS	1160	1395	665	835	1075	1295	920	1130	1535	2080	950	1350	1295	1775	1140	1590
2000RMS	1225	1470	675	850	1130	1360	955	1175	1630	2205	975	1390	1370	1880	1190	1665
2500RMS	1335	1605	695	875	1225	1475	1015	1245	1790	2425	1020	1460	1505	2065	1285	1800
3000RMS	1540	1855	720	910	1400	1690	1105	1370	2120	2875	1085	1565	1765	2425	1445	2040

SPB – Single Point Bonding; CB – Cross-bonding Both-ends; BE – Both-ends bonding

2.1 Technical data
Circuit-breakers for fixed installation and on withdrawable part

Rated voltage	kV	36 / 40.5	36 / 40.5
Rated frequency	Hz	50/60	50/60
Rated lightning impulse withstand voltage	kV	190	200[7]
Rated power frequency withstand voltage	kV	95	95
Rate of rise of transient recovery voltage	kV/µs	0.57 / 0.69	0.57 / 0.69
Peak of ransient recovery voltage	kV	62 / 70	62 / 70
Rated operating sequence		O-3min-CO-3min-CO	
Rated operating sequence with auto-reclosing		O-0.3s-CO-3min-CO	

Breaker type	Rated voltage	Rated current	Rated short-circuit breaking current symm. [1]	Rated short-circuit breaking current asymm. [1]	Rated short-circuit breaking current (peak) [1]	Rated short-circuit duration	Poles centres		Weight		Permissible operating cycles of the vacuum interrupters
							fixed	with-drawable	fixed	with-drawable	
VD4..	kV	A	kA	kA	kA	s	mm		approx. kg		Fig. 2/1 page 9/10
3606-16	36	630 [3]	16	17.4	40	4	360	280	320	290	Diagram A
3612-16	36	1250 [3]							320	290	Diagram A
3606-20	36	630 [3]	20	21.8	50	4	360	280	320	290	Diagram B
3612-20	36	1250 [3]							320	290	Diagram B
3612-25	36	1250 [3]	25	27.3	63	4	360	280	320	290	Diagram C
3616-25	36	1600 [3]							320	290	Diagram C
3620-25	36	2000 [3]							355	340	Diagram C
3625-25	36	2500 [4] [5]							355	340	Diagram C
3631-25	36	3150 [6]				3		280		290	Diagram F
3612-31	36	1250 [3]	31.5	34.3	80	4	360	280	320	290	Diagram D
3616-31	36	1600 [3]							320	290	Diagram D
3620-31	36	2000 [3]							355	340	Diagram D
3625-31	36	2500 [4] [5]							355	340	Diagram D
3631-31	36	3150 [6]				3		280		290	Diagram G
3612-40	36	1250 [3] [7]	40	43.6	100	4	360	280	330	300	Diagram E
3616-40	36	1600 [3] [7]							330	300	Diagram E
3620-40	36	2000 [3] [7]							365	350	Diagram E
3625-40	36	2500 [4] [5] [7]							365	350	Diagram E
4006-16	40.5	630 [3]	16	17.4	40	4	360	280	320	290	Diagram A
4012-16	40.5	1250 [3]							320	290	Diagram A
4006-20	40.5	630 [3]	20	21.8	50	4	360	280	320	290	Diagram B
4012-20	40.5	1250 [3]							320	290	Diagram B
4012-25	40.5	1250 [3]	25	27.3	63	4	360	280	320	290	Diagram C
4016-25	40.5	1600 [3]							320	290	Diagram C
4020-25	40.5	2000 [3]							355	340	Diagram C
4025-25	40.5	2500 [4] [5]							355	340	Diagram C
4031-25	40.5	3150 [6]				3		280		290	Diagram F
4012-31	40.5	1250 [3]	31.5	34.3	80	4	360	280	320	290	Diagram D
4016-31	40.5	1600 [3]							320	290	Diagram D
4020-31	40.5	2000 [3]							355	340	Diagram D
4025-31	40.5	2500 [4] [5]							355	340	Diagram D
4031-31	40.5	3150 [6]				3		280		290	Diagram G
4012-40	40.5	1250 [3] [7]	40	43.6	100	4	360	280	330	300	Diagram E
4016-40	40.5	1600 [3] [7]							330	300	Diagram E
4020-40	40.5	2000 [3] [7]							365	350	Diagram E
4025-40	40.5	2500 [4] [5] [7]							365	350	Diagram E

Guideline values for function times at the rated supply voltage:

Closing time	approx.	60 ms
Opening time	≤	45 ms
Arcing time (at 50 Hz)	≤	15 ms
Total break time	≤	60 ms
Minimum command time on closing	20 ms	(120 ms[2])
Minimum command time on opening	20 ms	(80 ms[2])

[1] When the operating voltage is lower than the rated voltage the same values apply as for rated voltage. Higher values on request.

[2] If the activating relay contact cannot itself interrupt the release coil current

[3] Ambient temperature ≤ 55 °C

[4] Ambient temperature ≤ 40 °C

[5] Rated current 2500 A at 55 °C ambient temperature (VD4 with forced ventilation (fan cooling) and assembled poles on withdrawable part)

[6] Rated current 3150 A at 40 °C ambient temperature (VD4 with forced ventilation (fan cooling) and assembled poles on withdrawable part)

[7]

Closing time	approx. 60 ms
Opening time	≤ 60 ... 90 ms
Arcing time (at 50 Hz)	≤ 15 ms
Total break time	≤ 75 ... 105 ms
Minimum command time on closing	20 ms (120 ms[2])
Minimum command time on opening	60 ms
Minimum command time on opening, if the activating relay cannot itself interrupt the release coil current	120 ms

2.4 Permissible number of vacuum interrupter operating cycles in relation to breaking current

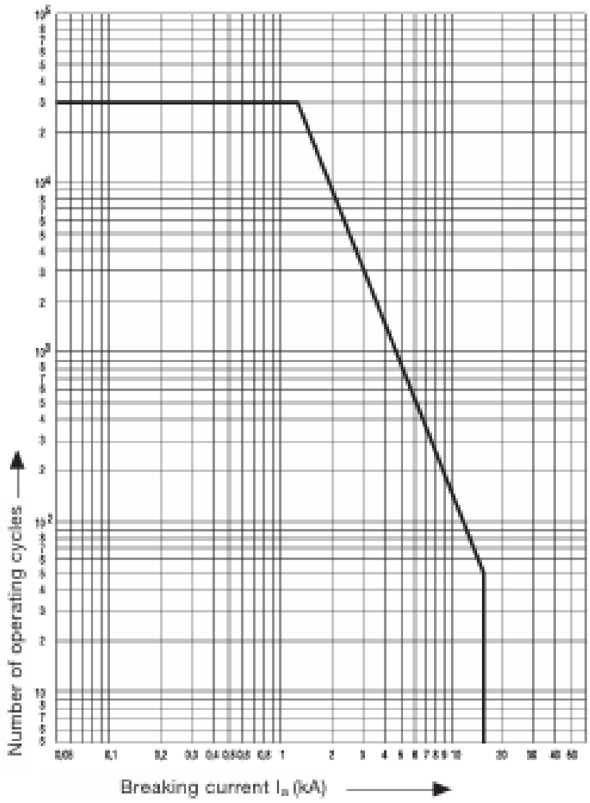

Diagram A)

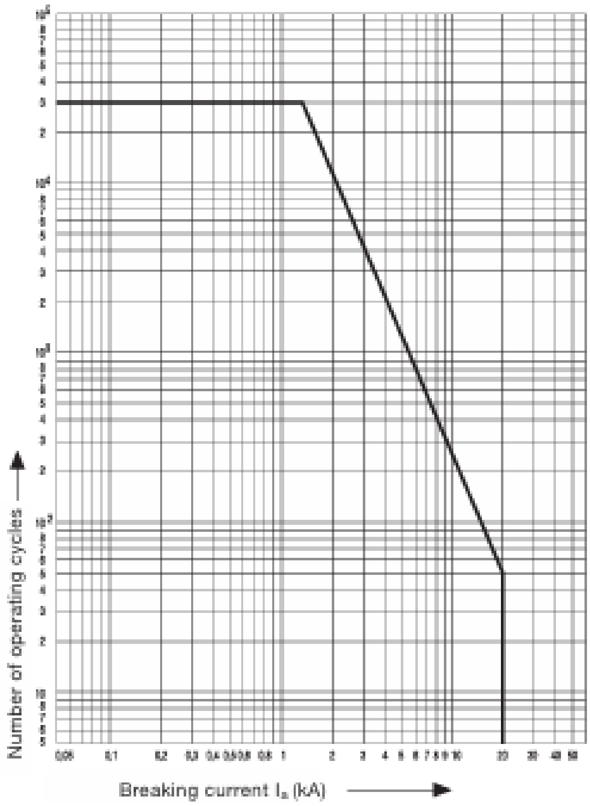

Diagram B)

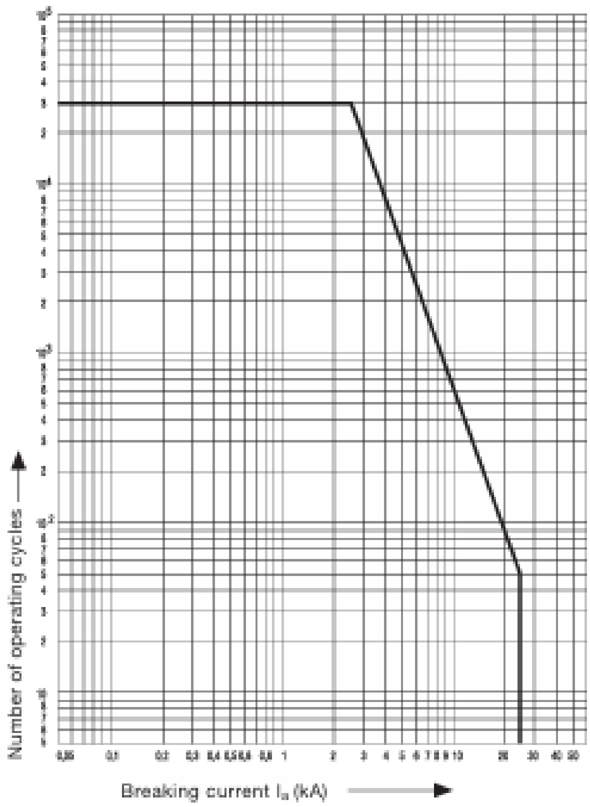

Diagram C)

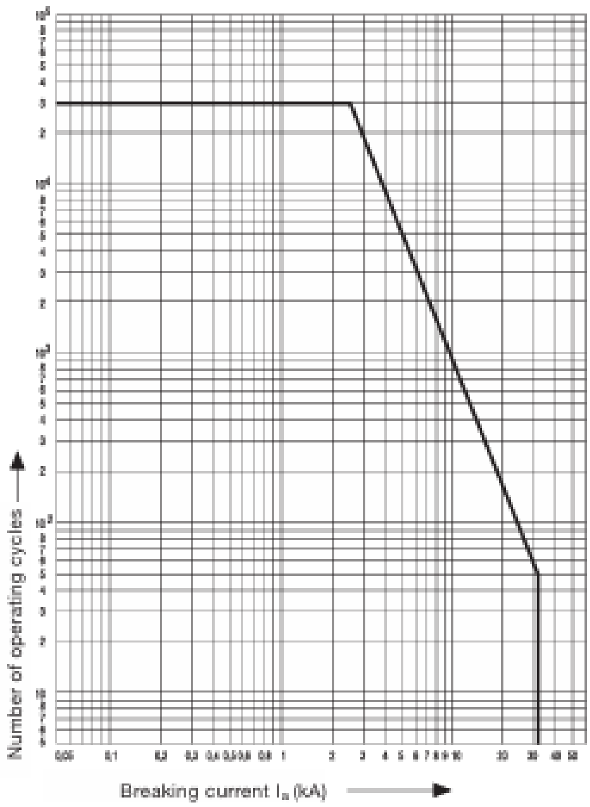

Diagram D)

Figure 2/1: Permissible number of vacuum interrupter operating cycles n as a function of the breaking current I_a.

Bibliography

[1] R. D. Evans, A. C. Monteith, and R. L. Witzke. “Power-System Transients Caused by Switching and Faults”. In: *Transactions of the American Institute of Electrical Engineers* 58.8 (1939), pp. 386–397. DOI: 10.1109/T-AIEE.1939.5057978.

[2] S. Dumronggittigule and K. Ngamsanroaj. “Thailand Experiences in Overvoltage Analysis and Events in Electric Power Transmission System due to Switching and Lightning Surges”. In: *2006 International Conference on Power System Technology*. 2006, pp. 1–7. DOI: 10.1109/ICPST.2006.321709.

[3] Bo Niu et al. “Study on Switching Transient and Influencing Factors of 330kV Cable Transmission System”. In: *2024 IEEE 2nd International Conference on Power Science and Technology (ICPST)*. 2024, pp. 342–346. DOI: 10.1109/ICPST61417.2024.10601978.

[4] Oktay Arikan, Celal Kocatepe, and Recep Yumurtaci. “Analysis of harmonics influences on load switching transients in simple power system”. In: *2008 Power Quality and Supply Reliability Conference*. 2008, pp. 169–173. DOI: 10.1109/PQ.2008.4653755.

[5] Juan Segundo-Ramirez et al. “Frequency Domain Methods for Accuracy Assessment of Wideband Models in Electromagnetic Transient Stability Studies”. In: *IEEE Transactions on Power Delivery* 35.1 (2020), pp. 71–83. DOI: 10.1109/TPWRD.2019.2927171.

[6] Sunil Subedi et al. “Review of Methods to Accelerate Electromagnetic Transient Simulation of Power Systems”. In: *IEEE Access* 9 (2021), pp. 89714–89731. DOI: 10.1109/ACCESS.2021.3090320.

[7] Transformers and Switchgear Committee. “IEEE Guide to Describe the Occurrence and Mitigation of Switching Transients Induced by Transformers, Switching Device, and System Interaction”. In: *IEEE Std C57.142-2010* (2011), pp. 1–56. DOI: 10.1109/IEEESTD.2011.5759579.

[8] W. Long et al. “EMTP-a powerful tool for analyzing power system transients”. In: *IEEE Computer Applications in Power* 3 (1990), pp. 36–41. DOI: 10.1109/67.56581.

[9] Dai Gao-jie. “Modeling and Simulation of Power System Based on EMTP”. In: *Journal of Luoyang Institute of Science and Technology* (2010).

[10] H. Ebrahimian, H. K. Hoidalen, and H. Nouri. “Statistical assessment of vacuum circuit breaker-induced transients in power transformers”. In: *IEEE Transactions on Power Delivery* 29.5 (2014), pp. 2281–2289. DOI: 10.1109/TPWRD.2014.2315712.

[11] Ebru Tavukcu and Belgin Emre Turkay. “Transient stability analysis of the transmission system considering the initial steady state results”. In: *International Symposium on Advanced Topics in Electrical Engineering (ATEE)*. IEEE, 2017, pp. 758–763. DOI: 10.1109/ATEE.2017.7905054. URL: https://ieeexplore.ieee.org/document/7905054/.

[12] J. Kosmac and P. Zunko. “A Statistical Vacuum Circuit Breaker Model for Simulation of Transient Overvoltages”. In: *IEEE Transactions on Power Delivery* 10.1 (1995), pp. 294–300. DOI: 10.1109/61.368386. URL: https://ieeexplore.ieee.org/document/368386.

[13] Allan Greenwood and Amos Selzer. “Electrical Transients in Power Systems”. In: *IEEE Transactions on Systems, Man, and Cybernetics* SMC-3.3 (1973), pp. 301–302. DOI: 10.1109/TSMC.1973.4309230.

[14] Lou van der Sluis. *Transients in Power Systems*. semanticscholar, 2001.

[15] N. Ari and W. Blumer. “Transient Electromagnetic Fields Due to Switching Operations in Electric Power Systems”. In: *IEEE Transactions on Electromagnetic Compatibility* EMC-29.3 (1987), pp. 233–237. DOI: 10.1109/TEMC.1987.304373.

[16] C. Hwang and J. N. Lou. “Transient analysis of capacitance switching for industrial power system by PSpice”. In: *Electr. Power Syst. Res.* 45.1 (1998), pp. 29–28. DOI: 10.1016/S0378-7796(98)00007-9.

[17] J. R. Marti, H. W. Dommel, and L. Linares. “Computation of electromagnetic transients”. In: *Proceedings of the IEEE* 92.5 (2004), pp. 1205–1225. DOI: 10.1109/JPROC.2004.826999.

[18] C. R. Paul. *Introduction to Electromagnetic Compatibility*. 2nd. Wiley, 2006. ISBN: 978-0471755005.

[19] B. Gustavsen and A. Semlyen. "Rational approximation of frequency domain responses by vector fitting". In: *IEEE Transactions on Power Delivery* 14.3 (1999), pp. 1052–1061. DOI: 10.1109/61.772353.

[20] B. Gustavsen. "Wide band modeling of power transformers". In: *IEEE Transactions on Power Delivery* 23.3 (2008), pp. 1434–1441. DOI: 10.1109/TPWRD.2007.916125.

[21] J. Christian and A. J. Moses. "Comparison of transformer models for electromagnetic transient studies". In: *IEEE Transactions on Power Delivery* 16.4 (2001), pp. 798–804. DOI: 10.1109/61.956718.

[22] J. Mahseredjian et al. "A new phase-coordinates transformer model for EMTP". In: *IEEE Transactions on Power Delivery* 22.1 (2007), pp. 144–150. DOI: 10.1109/TPWRD.2006.881449.

[23] H. K. Hoidalen and S. Olsen. "High-frequency modeling of power transformers by the finite element method and equivalent circuits". In: *IEEE Transactions on Power Delivery* 16.2 (2001), pp. 139–144. DOI: 10.1109/61.915507.

[24] C. R. Paul. *Analysis of Multiconductor Transmission Lines*. Wiley-Interscience, 2007.

[25] B. Gustavsen and A. Semlyen. "Simulation of transmission line transients using vector fitting and modal decomposition". In: *IEEE Transactions on Power Delivery* 8.2 (1993), pp. 620–629. DOI: 10.1109/61.216874.

[26] L. Marti. "Simulation of Transients in Underground Cables with Frequency-Dependent Modal Transformation Matrices". In: *IEEE Transactions on Power Apparatus and Systems* PAS-101.6 (1982), pp. 2399–2409. DOI: 10.1109/TPAS.1982.317547.

[27] B. Gustavsen and A. Semlyen. "Simulation of Transmission Line Transients Using the Universal Line Model". In: *IEEE Transactions on Power Delivery* 6.4 (1991), pp. 1573–1582. DOI: 10.1109/61.97686.

[28] C. H. Flurscheim. *Power Circuit Breaker Theory and Design*. IET, 1985. ISBN: 9780863410436.

[29] B. Gupta and A. Kumar. "Analysis of Re-strike Phenomenon in Vacuum Circuit Breakers for High-Frequency Applications". In: *IEEE Transactions on Dielectrics and Electrical Insulation* 22.5 (2015), pp. 3121–3128.

[30] emTP Software. *emTP Software Guide*. Version X.X. Retrieved from [URL if applicable]. Publisher/Organization, 20XX.

[31] A. A. Eajal, K. P. Schneider, and J. C. Fuller. "Machine learning-based methods for estimating and mitigating transient overvoltages in power systems". In: *Electric Power Systems Research* 189 (2020), p. 106785. DOI: 10.1016/j.epsr.2020.106785.

[32] M. F. Firuzabad and M. Shahidehpour. "Probabilistic modeling of capacitor bank switching transients in distribution networks". In: *IEEE Transactions on Power Delivery* 20.2 (2005), pp. 1010–1017. DOI: 10.1109/TPWRD.2004.843446.

[33] P. K. Sadhu and N. K. Roy. "Mitigation of transient overvoltage using hybrid damping techniques in modern power systems". In: *IET Generation, Transmission & Distribution* 14.20 (2020), pp. 4335–4343. DOI: 10.1049/iet-gtd.2019.1711.